
LATMiX: Learnable Affine Transformations for Microscaling Quantization of LLMs

Ofir Gordon¹ Lior Dikstein¹ Arnon Netzer¹ Idan Achituve^{*1} Hai Victor Habi^{*1}

Abstract

Post-training quantization (PTQ) is a widely used approach for reducing the memory and compute costs of large language models (LLMs). Recent studies have shown that applying invertible transformations to activations can significantly improve quantization robustness by reducing activation outliers; however, existing approaches are largely restricted to rotation or Hadamard-based transformations. Moreover, most studies focused primarily on traditional quantization schemes, whereas modern hardware increasingly supports the microscaling (MX) data format. Attempts to combine both showed severe performance degradation, leading prior work to introduce assumptions on the transformations. In this work, we take a complementary perspective. First, we provide a theoretical analysis of transformations under MX quantization by deriving a bound on the quantization error. Our analysis emphasizes the importance of accounting for both the activation distribution and the underlying quantization structure. Building on this analysis, we propose LATMiX, a method that generalizes outlier reduction to learnable invertible affine transformations optimized using standard deep learning tools. Experiments show consistent improvements in average accuracy for MX low-bit quantization over strong baselines on a wide range of zero-shot benchmarks, across multiple model sizes.

1. Introduction

Large language models (LLMs) have become a foundational component in a wide range of applications, including natural language understanding, code generation, reasoning, and multimodal systems (Brown et al., 2020; Chen, 2021; Alayrac et al., 2022; Wei et al., 2022a). Recent years have witnessed a rapid increase in both the scale and ca-

pability of these models, leading to substantial gains in performance and generalization ability (Kaplan et al., 2020; Hoffmann et al., 2022; Zhao et al., 2023). However, this scaling trend comes at a significant computational and memory cost, making efficient deployment increasingly challenging. Post-training quantization (PTQ) (Gholami et al., 2022) has therefore emerged as a key technique for reducing inference latency, memory footprint, and energy consumption while preserving model accuracy, without requiring expensive re-training (Lin et al., 2016; Nagel et al., 2020). As a result, a rich body of work has proposed diverse PTQ methods for LLMs, demonstrating that carefully designed quantization strategies can substantially lower deployment costs with mild performance degradation (Dettmers et al., 2022; Frantar et al., 2023; Xiao et al., 2023).

However, existing PTQ methods for LLMs often struggle in severely resource-constrained settings that require low bit widths, such as 4-bit quantization, where accuracy degradation becomes more pronounced. A key factor limiting performance in this regime is the presence of activation outliers, which dominate quantization error and prevent effective low-precision representation. Motivated by the intuition that redistributing energy more evenly across dimensions improves quantization robustness, several recent works mitigate activation outliers using invertible transformations, most notably rotation-based methods (Chee et al., 2023; Ashkboos et al., 2024c; Liu et al., 2025).

In parallel, new data formats have emerged, such as the microscaling (MX) format, introduced by the Open Compute Project (Rouhani et al., 2023b). The MX format is specifically designed to better accommodate the numerical characteristics of large models and is endorsed by Microsoft, AMD, Arm, Intel, Meta, and NVIDIA. The key idea behind MX is to partition the tensors into blocks, where each block is assigned its own scaling factor that can be dynamically selected (Rouhani et al., 2023a). This allows finer-grained control over the quantization error. The fine-grained scale enables both efficient training (Chmiel et al., 2025) and inference (Lee et al., 2025a) using MX quantization.

However, recent studies have shown that naively combining MX quantization with global rotation- or Hadamard-based transformations leads to severe performance degradation

^{*}Equal contribution ¹Arm Inc. Correspondence to: Hai Victor Habi <haivictor.habi@arm.com>.

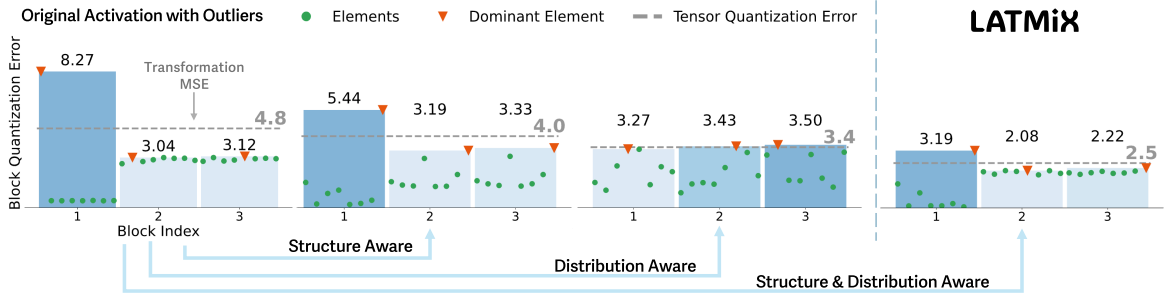


Figure 1. LATMiX takes into account both the MX block structure and the distribution of features to diffuse outliers. In the figure, energy is distributed both within the block and among blocks to obtain lower quantization error.

(Egiazarian et al., 2025; Shao et al., 2025). As a workaround, these studies suggest to apply such transformations independently within each MX block using block-diagonal rotation matrices. While this design choice avoids the immediate mismatch between global transformations and block-wise scaling, it fundamentally restricts the transformation to operate on small, isolated subspaces, preventing cross-block redistribution of activation mass. As a result, dominant outliers cannot be effectively diffused across the full tensor, limiting outlier suppression and leading to suboptimal quantization accuracy in low-bit regimes.

In this study, we address this gap by first presenting a theoretical and numerical analysis showing that quantization error depends on both the *feature distribution* and the *MX block structure*, with block-diagonal matrices representing only a special case. To more generally account for both factors, we propose LATMiX. Specifically, we define the class of admissible transformations as all invertible affine transformations, without imposing independence assumptions. The transformations are learned by optimizing free-form parameters corresponding to LU and QR decompositions of general invertible matrices, using a distillation loss and a volume-preserving regularization. The former encourages the predictions of the transformed quantized model to match those of the full-precision model, while the latter maintains invertibility throughout optimization. Since the learned transformations can be folded into the linear layers, they incur no additional inference cost when biases are present in the LLM, and only negligible overhead when biases are absent. This enables a substantially richer family of transformations, allowing more effective redistribution of activation mass and improved outlier mitigation.

To summarize, in this study we make the following novel contributions: (1) We conduct a theoretical and numerical study of MX quantization, emphasizing the importance of both the block structure and feature distribution; (2) We propose LATMiX, a method for learning affine transformations that can be folded into weight matrices based on LU and QR parameterizations; (3) We present experimental results on seven zero-shot reasoning benchmarks and WikiText2

using various LLM models. Across all evaluations LATMiX shows consistent improvements over leading baselines.

2. Background & Notation

We use bold lowercase letters to denote vectors (e.g., \mathbf{x}) and bold uppercase letters to denote matrices (e.g., \mathbf{W}). For notational convenience, and without loss of generality, when not written explicitly we assume that vectors lie in \mathbb{R}^d and matrices in $\mathbb{R}^{d \times d}$. Throughout the paper, \mathbf{x} is used as a generic notation for neural network activations.

2.1. Microscaling (MX) Quantization

Here we briefly outline MX quantization (Rouhani et al., 2023b), focusing on block-wise power-of-two dynamic scaling commonly used in conjunction with low-precision element formats such as FP4. In standard tensor-wise quantization, using one shared scale for an entire tensor can be suboptimal when values vary widely in magnitude. MX quantization addresses this by partitioning the tensor into small blocks, each of which is assigned its own scale factor rather than sharing a single global scale. More formally, let $\mathbf{x} \in \mathbb{R}^d$ be the vector to be quantized, B the MX block size, and $N_B = d/B$ the number of blocks (assuming B divides d). The quantization of an element \mathbf{x}_j belonging to block $i \in \{0, \dots, N_B - 1\}$ is defined as:

$$\begin{aligned} \text{Compute scale: } s_i &= 2^{\left\lfloor \log_2 \left(\max_{j \in \mathcal{I}_i} |\mathbf{x}_j| \right) \right\rfloor - r_{\max}}, \\ \text{Quantize: } Q(\mathbf{x})_j &= s_i Q_e \left(\frac{\mathbf{x}_j}{s_i} \right), \end{aligned} \quad (1)$$

where $\mathcal{I}_i = [i \cdot B, \dots, (i+1) \cdot B - 1]$ denotes the index set of the i^{th} block, $Q_e(\cdot)$ is the element-wise quantizer corresponding to the chosen low-precision format (e.g., FP8, INT4, FP4), and r_{\max} denotes the maximum exponent representable in that format. Throughout this work, we denote by $Q(\mathbf{x})$ the MX quantization operator defined in Eq. (1) applied on to the entire tensor \mathbf{x} .

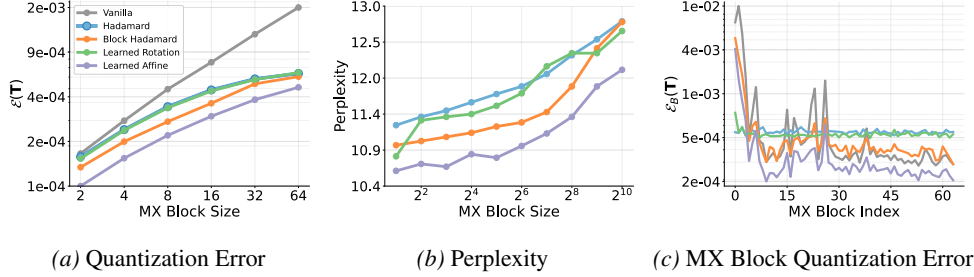


Figure 2. Analysis of various transformation types: (1) Vanilla: no transformation applied; (2) Hadamard: Full Hadamard transform; (3) Block Hadamard: a block-diagonal matrix in which each block corresponds to an MX block with an Hadamard matrix; (4) a learned rotation matrix; and (5) a learned affine transformation that minimizes the objective in Eq. (2). In Fig. 2a, the Hadamard and learned rotation curves are superimposed.

2.2. Outlier Reduction Using Rotation Matrices

In the literature, it has been observed that rotating the activations of a neural network (NN) prior to quantization helps reduce outliers, thereby lowering the quantization error (Tseng et al., 2024; Ashkboos et al., 2024c; Liu et al., 2025). Rotation transformations, as a subset of invertible linear transformations, are typically chosen in order to preserve computational invariance (Ashkboos et al., 2024a), namely, that the network with rotated activations remains functionally equivalent to the original network. This invariance is achieved by injecting the inverse transformation into the network after rotating the activations. More formally, consider a linear layer with activation \mathbf{x} , a weight matrix \mathbf{W} , and a rotation matrix \mathbf{A} , then, $\mathbf{x}^\top \mathbf{W} = (\mathbf{A}\mathbf{x})^\top (\mathbf{A}^{-\top} \mathbf{W})$.

Recently, it was proposed in (Liu et al., 2025) to learn the rotation matrices from a small calibration set, departing from previous approaches which set it in advance to some value. During the optimization process, weights are kept in full precision, while only the rotated activations are quantized. After learning the rotation matrices, the corresponding transformed weights are quantized as well. However, the approach proposed in (Liu et al., 2025) is restricted to rotation matrices only, and the optimization, which is performed directly on the Stiefel manifold, can be less amenable to common deep learning optimization techniques (Li et al., 2020; Huang et al., 2023). Furthermore, recent studies (Egiazarian et al., 2025; Shao et al., 2025) have shown that when MX quantization is applied to rotated activations, the outlier suppression can be severely harmed, resulting in substantial performance degradation. Hence, these studies suggested applying the rotations separately per MX block.

3. Method

We first conduct a theoretical and numerical study of quantization error under various transformations in MX quantization. Our findings show that both the activation distribution and the MX block structure play a crucial role in designing

transformations that effectively reduce quantization error. Building on this analysis, we introduce LATMiX, a method that learns from the class of invertible affine transformations. An illustration of the proposed approach is shown in Fig. 1.

3.1. Theoretical & Numerical Analysis

Here, we provide a theoretical and numerical analysis of the transformation effect on the microscaling quantization error. We begin by defining the affine transformation \mathbf{T} , its inverse and the MSE error under MX quantization.

Definition 3.1 (General Affine Transformation). Let $\mathbf{A} \in \mathbb{R}^{d \times d}$ be an invertible matrix and \mathbf{v} be a translation vector. Then an affine transformation is defined as $\mathbf{T}(\mathbf{x}) = \mathbf{A}\mathbf{x} + \mathbf{v}$ and its inverse $\mathbf{T}^{-1}(\mathbf{y}) = \mathbf{A}^{-1}\mathbf{y} - \mathbf{A}^{-1}\mathbf{v}$.

To examine various types of transformations, we employ the Mean Squared Error (MSE), which approximates changes in the objective function induced by perturbations in weights and activations (Nagel et al., 2020; Gordon et al., 2024).

Definition 3.2 (Transformation Mean Squared Error). The Transformation Mean Squared Error for \mathbf{T} is defined as:

$$\mathcal{E}(\mathbf{T}) \triangleq \frac{1}{d} \mathbb{E} \left[\|\mathbf{x} - \mathbf{T}^{-1}(Q(\mathbf{T}(\mathbf{x})))\|_2^2 \right], \quad (2)$$

where $\|\cdot\|_2$ denotes the Euclidean norm of a vector.

Theoretical Analysis. We first derive an upper bound for the quantization error defined in Eq. 2 for general distributions, and then present its concrete form in the case of sub-Gaussian distributions, allowing us to draw practical insights. The class of sub-Gaussian distributions is broad; in particular, any centered random variable with bounded support is sub-Gaussian (Vershynin, 2018). As our interest lies in extreme-value behavior, sub-Gaussian distributions are well suited due to their Gaussian-dominated tails.

Theorem 3.3 (MX Quantization Error). Assume that \mathbf{x} is a continuous random vector, \mathbf{T} is an affine transformation and Q is the quantization of MX as defined in Eq. (1). Then,

under regularity assumptions on \mathbf{x} ,

$$\mathcal{E}(\mathbf{T}) \lesssim \frac{\|\mathbf{A}^{-1}\|_\sigma^2}{N_B} \sum_{i=1}^{N_B} M_i, \quad \text{where} \quad (3)$$

$$M_i \triangleq \mathbb{E} \left[\left(\max_{j \in \mathcal{I}_i} |[\mathbf{T}(\mathbf{x})]_j| \right)^2 \right].$$

Here, $f(x) \lesssim g(x)$ denotes that $f(x)$ is less than $g(x)$ up to a fixed multiplicative constant, and $\|\cdot\|_\sigma$ denotes the spectral norm. Furthermore, if we assume that \mathbf{x} is a sub-Gaussian random vector with mean $\boldsymbol{\mu}$ then,

$$M_i \lesssim \left(\mathbf{T}_{\max}(\boldsymbol{\mu}) + (\log(B))^{1/2} \max_{j \in \mathcal{I}_i} \left\| \left[\hat{\mathbf{T}}(\mathbf{x}) \right]_j \right\|_{\psi_2} \right)^2. \quad (4)$$

Where $\|z\|_{\psi_2} \triangleq \inf \left\{ K > 0 : \mathbb{E} \left[\exp \left(\frac{z^2}{K^2} \right) \right] \leq 2 \right\}$ is the Sub-Gaussian norm of the random variable z , $\mathbf{T}_{\max}(\mathbf{x}) \triangleq \max_{j \in \mathcal{I}_i} |[\mathbf{T}(\mathbf{x})]_j|$, and $[\hat{\mathbf{T}}(\mathbf{x})]_j \triangleq [\mathbf{T}(\mathbf{x}) - \mathbf{T}(\boldsymbol{\mu})]_j$.

From Theorem 3.3 (see the proof in Appendix A), we see that the MSE is determined by two factors: (1) the norm $\|\mathbf{A}^{-1}\|_\sigma^2$, and (2) the average, across MX blocks, of the expected maximum absolute channel value within each block. Reducing either term leads to a lower transformation MSE. However, these factors can be at odds. Reducing the first term, by increasing the smallest singular value of \mathbf{A} , may increase $\sum_{i=1}^{N_B} M_i$, while transformations that reduce this sum can simultaneously reduce the smallest singular value, thereby increasing $\|\mathbf{A}^{-1}\|_\sigma^2$. The existence of this tradeoff hints that learning the transformation is required to navigate and balance between the terms.

Furthermore, Eq. (3) provides key insights into the design of the transformation \mathbf{T} . In particular, choosing \mathbf{A} as a random invertible matrix can be detrimental, as indiscriminate channel mixing may increase quantization error. To illustrate, consider a length-four vector with a Dirac delta distribution centered at $[10, 1, 0.5, 0.5]$, and an MX block size of $B = 2$. Applying the Walsh–Hadamard matrix $\mathbf{T} = \mathbf{H}_4$ yields the rotated vector $[6, 4.5, 5, 4.5]$, which reduces the error in the first block but increases it in the second block. Motivated by such behavior, prior work (Egiazarian et al., 2025; Shao et al., 2025) advocates the use of block-diagonal transformations. This choice is supported by Eq. (3): owing to the additive structure of the bound, the error contribution of the i^{th} MX block depends on $\|\mathbf{A}_i^{-1}\|_\sigma^2 M_i$, where \mathbf{A}_i^{-1} denotes the submatrix corresponding to block i . Operating on each block independently can therefore reduce the per-block error and, consequently, the total error.

However, the block-diagonal approach implicitly assumes independence of the channels across blocks. As a result,

even if the average per-block error decreases, the overall error may remain large. To address both sources of error, we argue for using full (non-block-diagonal) transformations that explicitly account for both the MX block structure and the channel distribution. One way to account for both the MX structure and the data distribution is to learn the transformation coupled with MX quantization on activations. From cardinality considerations, as $O(d) \subset GL(d) \subset \text{Aff}(d)$, namely the group of orthogonal matrices is a subset of the general linear group which itself is a subset of the general affine group, then it immediately follows that $\min_{\mathbf{T} \in O(d)} \mathcal{E}(\mathbf{T}) \geq \min_{\mathbf{T} \in GL(d)} \mathcal{E}(\mathbf{T}) \geq \min_{\mathbf{T} \in \text{Aff}(d)} \mathcal{E}(\mathbf{T})$. Hence, we suggest to define the set of admissible transformations as the general affine group.

The benefit of adding the bias term, namely preferring $\text{Aff}(d)$ over $GL(d)$, is further corroborated when considering the sub-Gaussian case (Eq. (4)). If $\mathbf{T}(\boldsymbol{\mu}) = \mathbf{0}$ before quantization, then $\max_{j \in \mathcal{I}_i} |[\mathbf{T}(\boldsymbol{\mu})]_j|$ is eliminated from M_i . In principle, it can be obtained using the linearity of both the transformation and the expectation by setting the bias term according to $\mathbf{T}(\boldsymbol{\mu}) = \mathbf{A}\boldsymbol{\mu} + \mathbf{v} = \mathbf{0} \Rightarrow \mathbf{v} = -\mathbf{A}\boldsymbol{\mu}$.

We note that while prior studies (Egiazarian et al., 2025; Shao et al., 2025) empirically investigated learning full transformations using the method proposed in Liu et al. (2025), which was not developed in the context of MX quantization, there are two important distinctions from our approach. First, the transformations in these studies are restricted to the set $O(d)$, whereas we consider the broader class $\text{Aff}(d)$. Second, the optimization procedure differs, as we optimize over free-form matrices and use a distillation loss instead of a cross-entropy loss. We discuss both points in detail in Section 3.2. These design choices can have a significant empirical impact, as demonstrated in Section 5, but first we analyze them numerically.

Numerical Analysis. To further illustrate Theorem 3.3, we evaluate several common transformations in a numerical study. Figure 2 reports quantization error and perplexity on features from Llama3.2-1B. Figure 2a shows the transformation MSE as a function of the MX block size. As expected, the quantization error increases with block size for all methods. Moreover, for smaller block sizes, full and block-wise Hadamard transformations perform similarly, with a slight advantage for the full Hadamard. We hypothesize that since outliers are typically confined to a small number of channels (Liu et al., 2025), smaller blocks allow the Hadamard transformation to spread these outliers across more blocks, reducing the overall error. In addition, learning rotation matrices using the approach proposed in (Liu et al., 2025) is comparable to using random Hadamard matrix. Fig. 2b further presents the perplexity for various block sizes, and Fig. 2c shows the block-wise quantization error defined as, $\mathcal{E}_B^i(\mathbf{T}) \triangleq \frac{1}{B} \sum_{j \in \mathcal{I}_i} ([\mathbf{x} - \mathbf{T}^{-1}(Q(\mathbf{T}(\mathbf{x})))]_j)^2$. From

Fig. 2c, we observe that, compared to the vanilla transformation, rotation-based transformations produce nearly uniform quantization error across blocks but increase the overall error for most of them. The block-Hadamard transformation reduces the error in the dominant (early-index) blocks, usually causing a minor increase in error for the remaining blocks. In contrast, the learned affine transform reduces the error across all blocks uniformly. Finally, across all the results, we observe that the learned affine transformations consistently outperform other approaches. This underscores the advantage of learning general affine transformations that consider both the MX block structure and the distribution of feature maps.

3.2. Learning General Affine Transformation

Our analysis in Section 3.1 reveals important design choices for constructing transformations that take into account both MX data format and the features distribution. Most notably, defining the set of admissible functions to be invertible affine transformations. This is in contrast to previous studies that restrict the set of invertible transformations, usually to rotation matrices only. We now introduce LATMiX, a method that uses and learns *general* invertible affine transformations for reducing activations outliers. We stress here two important aspects of LATMiX: (1) It does not incur additional computational costs at inference time compared to common rotation-based methods for models with bias terms ¹; (2) Although our approach was developed for MX data format, it can seamlessly be applied to other data formats.

We follow previous studies (Tseng et al., 2024; Ashkboos et al., 2024c; Liu et al., 2025) and define invertible transformations that can be absorbed into weight matrices, \mathbf{T}_1 and \mathbf{T}_2 , and an online transformation \mathbf{T}_3 (see Fig. 4 for an illustration). Specifically, \mathbf{T}_1 acts globally on the input activations of all transformer blocks, while \mathbf{T}_2 and \mathbf{T}_3 act locally per transformer block on the activations of the scaled dot-product layer in the attention layer and inside the feed-forward network, respectively. As in previous work (Liu et al., 2025; Egiuzarian et al., 2025; Shao et al., 2025) we learn \mathbf{T}_1 and \mathbf{T}_2 only; However, there are two important distinctions from prior studies, aside from the set of admissible invertible functions. First, we apply the optimization on free-form matrices followed by deterministic transformations. As a result, common deep learning optimization algorithms can be used instead of constrained optimization on manifolds (Liu et al., 2025). Second, we soften the requirement of functional equivalence between the unquantized network and the transformed network, allowing them to be approximately equivalent by optimizing a distillation loss. We discuss both points in detail next.

¹See Appendix C for further details; For models that have bias terms the additional cost from the addition is negligible.

Parametrization of the transformations. We start by introducing our approach to constructing invertible transformations. We present here two parameterizations for \mathbf{A} ; the first is inspired by (Kingma & Dhariwal, 2018) which uses LU decomposition, and the second uses QR decomposition. Starting with the former, \mathbf{A} is decomposed according to:

$$\mathbf{A} = \mathbf{P}\mathbf{L}(\mathbf{U} + \text{diag}(\mathbf{s})), \quad (5)$$

where $\text{diag}(\cdot)$ means constructing a diagonal matrix with \mathbf{s} on its diagonal, $\mathbf{P} \in \mathbb{R}^{d \times d}$ is a fixed permutation matrix, and the learned parameters are: $\mathbf{L} \in \mathbb{R}^{d \times d}$ a lower unitriangular matrix, $\mathbf{U} \in \mathbb{R}^{d \times d}$ an upper triangular matrix with zeros on its diagonal, and the vector $\mathbf{s} \in \mathbb{R}^d$. Although the LU parametrization gives good empirical results, it is limited in the class of invertible transformations it can represent. Hence, we suggest a parametrization based on QR decomposition which spans the entire GL group. Concretely,

$$\mathbf{Q} = \exp\left\{\frac{1}{2}(\mathbf{G} - \mathbf{G}^\top)\right\}; \quad \mathbf{A} = \mathbf{Q}(\mathbf{R} + \text{diag}(\mathbf{s})), \quad (6)$$

where $\exp(\cdot)$ is the matrix exponential and the learned parameters are $\mathbf{G} \in \mathbb{R}^{d \times d}$, $\mathbf{R} \in \mathbb{R}^{d \times d}$ an upper triangular matrix with zeros on the diagonal, and the vector $\mathbf{s} \in \mathbb{R}^d$. \mathbf{Q} is ensured to be orthogonal as the exponent operates on a skew-symmetric matrix, and $\mathbf{R} + \text{diag}(\mathbf{s})$ by design is an upper triangular matrix.

Using the parameterizations in Eq. 5 & 6, ensuring that \mathbf{A} is invertible amounts to enforcing that $\det(\text{diag}(\mathbf{s})) > 0$. We control it by initializing \mathbf{A} to be a block-diagonal rotation matrix and using the following regularization,

$$\mathcal{L}_{vol} = \left(\prod_{i=1}^d |s_i| - 1\right)^2. \quad (7)$$

As $|\det(\mathbf{A})| = \prod_i |s_i|$, this regularization essentially attempts to keep the absolute determinant of the transformation close to one, pushing the transformation to be volume preserving. The goal of the regularization is two-fold: (1) mitigate numerical instabilities; and (2) allowing individual directions to expand or contract while preserving the overall volume of the activation region. In practice, instead of learning \mathbf{s} directly, we learn $\log|\mathbf{s}|$ and regularize $(\sum_{i=1}^d \log|s_i|)^2$ to be close to zero. This objective shares the same minima as that in Eq. 7, but is more stable.

Learning the transformations. We now turn to describe the optimization procedure of LATMiX. Let $f(\cdot)$ denote the full-precision LLM with N transformer layers. Our goal is to learn $N + 1$ sets of parameters of the form $\{\mathbf{L}, \mathbf{U}, \mathbf{s}, \mathbf{v}\}$ for the LU parametrization and $\{\mathbf{G}, \mathbf{R}, \mathbf{s}, \mathbf{v}\}$ for the QR parametrization. One set for parameterizing \mathbf{T}_1 and N such sets, one for each transformer block, for parameterizing \mathbf{T}_2 . Denote by Ω the set of all learnable parameters and by $f_\Omega(\cdot)$

the corresponding network to $f(\cdot)$ with the activations transformed according to \mathbf{T}_1 and \mathbf{T}_2 and then quantized using MX. In the literature, orthogonal transformations are chosen to uphold the computational invariance theorem (Ashkboos et al., 2024a;c), as they do not modify the output of RMSNorm layers, namely $\frac{\mathbf{x}}{\|\mathbf{x}\|_2} = \mathbf{A}^{-1} \frac{\mathbf{Ax}}{\|\mathbf{Ax}\|_2}$. In our case, since we allow general invertible matrices, it is no longer true as \mathbf{A} does not have to be orthogonal and we have a bias term v . Hence, we relax this restriction by initializing \mathbf{T} to be a rotation transformation and learn Ω using a distillation loss on a small set of examples (Hinton et al., 2015),

$$\mathcal{L}_{dist} = \text{KL} \left(f(\mathbf{x}), \tilde{f}_{\Omega}(\mathbf{x}) \right). \quad (8)$$

Here, KL refers to Kullback-Leibler divergence, $f(\mathbf{x})$ is the teacher and $\tilde{f}_{\Omega}(\mathbf{x})$ is the student. At the start of training, the initialization enforces consistency between the models. During optimization, the loss allows traversing the transformation space to reach a better solution while approximately maintaining consistency between the models. Since common quantization methods (e.g., GPTQ) already rely on an unlabeled calibration set, we reuse a subset of these examples for the purpose of learning Ω as well and apply it to various tasks, including zero-shot tasks. To summarize, the final loss for learning Ω is $\mathcal{L} = \mathcal{L}_{dist} + \lambda \cdot \mathcal{L}_{vol}$, where λ is a hyper-parameter controlling the effect of the regularization. In our experiments, we found that LATMiX was extremely robust to the selection of λ . In Appendix E.3, we further compare the loss in Eq. 8 to per-block MSE loss, and theoretically connect it to standard next token prediction cross-entropy loss (Liu et al., 2025). We found that the KL loss is preferred in zero-shot settings over both alternatives, where the transformations are learned by solving a language modeling tasks and used for other tasks.

Weight quantization. After completing the optimization stage, the transformations \mathbf{T}_1 and \mathbf{T}_2 are folded into the linear operations of the model. A detailed description of the folding process is provided in Appendix C. A quantization procedure is then applied, such as GPTQ (Frantar et al., 2023), to compensate for weight quantization error.

4. Related Work

A prominent approach to reduce the inference cost in LLMs is post-training quantization (PTQ) (Lin et al., 2016; Nagel et al., 2020). In recent years, several studies proposed methods for quantizing transformer-based LMs, (Shen et al., 2020; Yao et al., 2022; Lee et al., 2023; Frantar et al., 2023), to name a few. Two central aspects of quantization are the numerical representation format of model elements (e.g., FP4, MXFP4), and the mitigation of outliers to reduce errors prior to quantization. In this study, we focus mainly on MX (Rouhani et al., 2023b) as it was shown to be highly effective for language models (Rouhani et al., 2023a).

As outliers are prominent in LLMs, many approaches were presented to tackle them. Several attempts used grouping and mixed precision quantization (Bondarenko et al., 2021; Dettmers et al., 2022; 2024; Ashkboos et al., 2024b; Kim et al., 2024; Zhao et al., 2024; Ramachandran et al., 2025), which limits their applicability in cases of hard constrained low-bit precision for all quantities and requires costly operations. Other approaches build on invertible transformations, such as reparameterizing activations and weights through shifting and scaling operations (Wei et al., 2022b; 2023; Shao et al., 2024), scaling the weights based on activations information (Xiao et al., 2023; Liu et al., 2023; Lin et al., 2024b), and multiplying the weights per-layer with random orthogonal (Chee et al., 2023), Hadamard (Tseng et al., 2024), and rotation (Ashkboos et al., 2024c) matrices to spread the magnitude and sensitivity across coordinates. LATMiX generalizes these approaches by allowing *general* affine transformation. Instead of using random rotations to mitigate outliers, several studies proposed different alternatives to construct and learn rotation matrices (Lin et al., 2024a; Liu et al., 2025; Akhondzadeh et al., 2025). Lin et al. (2024a) proposed using greedy search combined with permutation of (non-MX) blocks to obtain a balanced distribution of outliers. However, this method fails to account the MX block structure. Liu et al. (2025) proposed to learn rotation matrices on the Stiefel manifold. LATMiX instead learns free-form matrices, allowing us to use the full machinery of deep learning optimization (Kingma & Ba, 2015; Loshchilov & Hutter, 2019). The studies closest to ours are (Ma et al., 2024) and (Sun et al., 2025), which used invertible transformations, although not under MX quantization. In both (Ma et al., 2024) and (Sun et al., 2025), the transformations were restricted only to a subclass of all invertible matrices, namely strictly diagonally dominant matrices in the former and Kronecker product of lower rank matrices in the latter. Also, unlike LATMiX, both approaches learn only local matrices per transformer block online using a local loss. As a result, some transformations are limited to scaling transformation only (Ma et al., 2024), or are computationally more costly, as folding is not supported (Sun et al., 2025). In Section 5, we compare to the latter, showing a consistent benefit for LATMiX over it. Several studies have explored outlier reduction under MX quantization. Sharify et al. (2024) adapt GPTQ (Frantar et al., 2023) to the block-wise setting and combine it with SmoothQuant (Xiao et al., 2023) and AWQ (Lin et al., 2024b) for outlier reduction. Lee et al. (2025b) identified that rotation of activations and microscaling lack synergy and proposed a new format using asymmetric scales shared within a quantization group. Likewise, Lee et al. (2025a) proposed to modify the MX format by re-purposing the exponent field to store more mantissa bits. Unlike these studies, we focus on outlier mitigation without modifying the PTQ method or data format. Lastly, recently (Egiazarian et al., 2025) and (Shao et al., 2025)

Table 1. Zero-shot average accuracy (Acc.) and average recovery (Rec.) in percentages on seven commonsense and reading-comprehension benchmarks. All methods were evaluated under the same experimental setup. All methods except RTN and QuaRot-RTN were combined with GPTQ quantization scheme. Within each model, the best method is in **bold** and the second best is underlined.

Format	Method	Llama3.2-1B		Llama3.2-3B-Instruct		Llama3.1-8B-Instruct		Qwen3-1.7B		Qwen3-4B		Qwen3-8B	
		Acc.	Rec.	Acc.	Rec.	Acc.	Rec.	Acc.	Rec.	Acc.	Rec.	Acc.	Rec.
MXFP4	RTN	47.89	83.09	58.85	91.76	66.84	93.77	48.22	79.56	61.60	91.84	62.96	89.69
	QuaRot-RTN	48.24	83.38	55.15	86.00	57.52	80.46	45.70	75.47	59.74	88.66	61.91	87.86
	GPTQ	51.42	89.03	59.54	92.97	68.11	95.70	52.68	87.56	62.61	93.13	65.68	93.77
	QuaRot	52.47	91.09	59.90	93.98	67.64	94.95	52.71	88.11	61.31	91.00	66.47	94.91
	SpinQuant	51.48	89.20	60.14	93.89	68.23	95.65	53.53	88.55	61.85	92.04	66.96	95.74
	FlatQuant	52.45	90.54	60.55	94.73	67.80	94.92	54.85	90.98	62.46	92.96	66.89	95.34
	MR-GPTQ	52.53	90.89	60.89	95.37	<u>68.59</u>	<u>96.45</u>	52.59	87.34	62.05	92.02	67.57	96.51
	LATMiX-LU (Ours)	54.18	94.05	62.25	97.75	68.77	96.58	56.91	94.67	<u>63.74</u>	<u>95.03</u>	68.66	98.24
	LATMiX-QR (Ours)	<u>52.99</u>	<u>92.17</u>	<u>61.54</u>	<u>96.30</u>	68.37	96.02	<u>56.31</u>	<u>93.56</u>	64.03	95.33	<u>68.08</u>	<u>97.26</u>
MXINT4	RTN	45.14	78.14	54.58	85.45	64.25	89.81	44.11	72.98	51.06	76.47	59.17	84.23
	QuaRot-RTN	44.55	77.46	51.40	79.71	62.94	88.11	42.79	70.70	52.64	78.21	59.24	84.01
	GPTQ	49.06	85.00	59.25	92.72	62.08	86.82	48.47	80.42	57.00	85.78	62.08	88.40
	QuaRot	49.90	86.30	58.63	91.76	67.12	94.24	49.38	81.98	59.60	88.42	65.60	93.42
	SpinQuant	48.28	83.70	56.01	87.41	<u>67.81</u>	<u>95.39</u>	54.14	89.99	60.14	90.18	65.47	93.51
	FlatQuant	50.34	87.25	58.31	90.77	66.04	92.35	53.12	88.56	61.50	91.50	65.80	93.76
	MR-GPTQ	51.37	89.08	60.82	95.34	68.18	95.87	52.79	87.98	61.65	91.64	66.24	94.51
	LATMiX-LU (Ours)	53.16	92.40	61.10	95.46	67.75	94.90	<u>54.86</u>	<u>90.77</u>	<u>62.54</u>	<u>93.35</u>	67.04	95.77
	LATMiX-QR (Ours)	<u>51.84</u>	<u>90.38</u>	59.77	93.21	67.52	94.47	54.84	91.13	62.74	93.49	<u>66.64</u>	<u>95.09</u>

study quantization under the MX format. Both studies advocate for using block diagonal rotation matrices, instead of full rotation matrices. Our analysis shows that it indeed can be beneficial; however, different from these studies, we found that adopting and learning full affine transformations that account for the feature distribution and the MX block structure can mitigate outliers more effectively.

5. Experiments

We evaluate LATMiX performance on various language models and tasks to demonstrate its effectiveness. We conducted experiments on Llama3.2 (AI, 2024) (1B/3B) Llama3.1 (Dubey et al., 2024) (8B), and Qwen3 (Yang et al., 2025) (1.7B/4B/8B) models. We focus primarily on small-scale models, as our interest lies on regimes of extreme quantization. In the main text, we present results on 7 zero-shot commonsense reasoning tasks. Appendix E presents additional results and ablation studies, supporting different design choices for LATMiX, including perplexity on WikiText2 dataset (Merity et al., 2016) in Appendix E.1.

5.1. Experimental Settings

The optimization of LATMiX proceeds in two stages. First, invertible affine transformation are learned for T_1 and T_2 as described in Section 3.2. In the second stage, block-wise GPTQ is applied to the transformed weights similarly to previous studies (e.g., (Egiazarian et al., 2025)). We compare LATMiX against several methods spanning both MX quantization alone and MX combined with different transformation-based approaches for outlier suppression. We first evaluate MX quantization without transformations.

These experiments are denoted as **RTN** for plain round-to-nearest quantization, and as **GPTQ** when using GPTQ as the underlying quantization scheme. We then combine each method with tensor-wise or block-wise transformations to emulate prior approaches, including QuaRot (Ashkboos et al., 2024c), SpinQuant (Liu et al., 2025), FlatQuant (Sun et al., 2025) and MR-GPTQ (Egiazarian et al., 2025), and evaluate them on the same benchmarks. Transformations are learned using 256 samples from the WikiText2 dataset (Merity et al., 2016). All experiments were conducted using the codebase provided by (Egiazarian et al., 2025) with MX block size set to 32. We follow the implementation of (Liu et al., 2025) and execute all methods under the same experimental setup to ensure fairness in the comparisons. Appendix D provides full implementation details.

5.2. Zero-shot Reasoning Tasks Evaluation

We evaluate zero-shot accuracy on a suite of commonsense and reading-comprehension benchmarks: ARC (Easy and Challenge) (Clark et al., 2018), HellaSwag (Zellers et al., 2019), WinoGrande (Sakaguchi et al., 2021), PIQA (Bisk et al., 2020), BoolQ (Clark et al., 2019), and OpenBookQA (OBQA) (Mihaylov et al., 2018). All results are obtained using the LM Evaluation Harness (Gao et al., 2024) with default task settings. Performance is summarized in Table 1, where we report, for each quantized model, the mean accuracy and mean recovery relative to the floating-point baseline averaged across tasks. Full per-benchmark results are provided in Appendix F. From the table, consistent with prior work (Egiazarian et al., 2025; Shao et al., 2025), combining RTN with QuaRot leads to performance degradation. In addition, while learning the transformations as

Table 2. Transformation and granularity ablation on WikiText2.

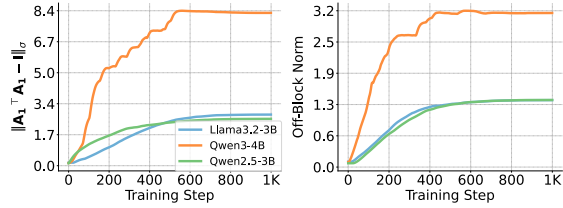
Transformation	Granularity	Llama3.2-1B	Qwen3-1.7B
None	-	18.80	21.29
Random Hadamard	Block	12.25	21.30
	Full	12.87	20.24
Learned Orth. Matrix (Ours)	Block	13.89	18.20
	Full	13.35	17.70
Learned Inv. Matrix (Ours)	Block	12.16	21.11
	Full	11.75	17.50
LATMiX-LU (Ours)	Block	12.08	18.13
	Full	11.69	16.98

in SpinQuant and FlatQuant or using block-wise transformations improve quantization performance, these methods remain limited and do not fully exploit the potential of transformation-based outlier suppression under MX quantization. In contrast, LATMiX achieves the best overall performance, indicating that explicitly accounting for both the MX quantization structure and the activation distribution via invertible affine transformations is more effective. Lastly, we observe a small advantage for the LU over QR parameterization, which we attribute to the optimization process of the QR, as it requires backpropagation through a matrix exponential. Appendix E.1 further reports perplexity results on WikiText2, showing that LATMiX outperforms baseline methods on that benchmark as well.

5.3. Ablation & Analysis

Transformation Type Analysis. To study the effect of different components in LATMiX, we evaluate the perplexity on WikiText2 of MXFP4-quantized models under different types of transformations for both T_1 and T_2 . We consider two baselines: (1) None - without transformations; and (2) Random Hadamard matrices. We also evaluate three variants of our approach: (3) Orthogonal transformations, learning only Q in the QR parametrization; (4) Invertible transformations, learning A only using LU decomposition; And (5) the LU variant of LATMiX. Each method is applied either at the tensor level (Full) or in a block-wise manner (Block). Results on WikiText2 perplexity are shown in Table 2. From the table, learning invertible transformations is preferred over both learnable orthogonal transformations and random rotations but is subpar to learning affine transformations. LATMiX applied at the tensor level consistently achieves the best performance across models. These findings indicate that learning both a general invertible linear transform and a bias term at full granularity is more effective than fixed rotations or block-wise alternatives for mitigating activation outliers. Moreover, we observe that block-wise Hadamard rotation outperforms full Hadamard rotation on Llama3.2-1B, while this trend does not hold for Qwen3-1.7B. This emphasizes that both the quantization structure and the feature distribution should be taken into account.

Learned Transformation Analysis. To better understand



(a) Orthogonal Distance (b) Off-Diagonal Norm

Figure 3. LATMiX learns a transformation that spreads the energy across the tensor.

the behavior of our learned transformation, we report two metrics in Fig. 3. Fig. 3a shows the orthogonality deviation of the learned transform matrix A_1 by measuring the distance from an orthogonal transformation using the spectral norm. Fig. 3b measures the spectral norm of the off-block-diagonal components of the learned transformation, achieved by assigning zeros to the block-diagonal elements. An increase in this metric suggests that the learned matrix departs from purely block-diagonal behavior, enabling interactions across blocks. From Fig. 3a, the orthogonality deviation increases rapidly during the early stages of training from the initialized orthogonal matrix. This indicates that the optimization quickly moves away from the orthogonal constraint. After this initial phase, the deviation stabilizes, suggesting convergence to a non-orthogonal but more effective solution for quantization. Furthermore, Fig. 3b shows that indeed the optimization adapts to the MX quantization structure, moving beyond intra-block outlier redistribution and allowing cross-block energy transfer. Additional analysis of the learned transformation deviation from the orthogonal initial point can be found in Appendix E.2.

6. Conclusion

In this work, we analyze the quantization error of the MX format and demonstrate the importance of incorporating both structural knowledge and feature distributions. Building on this analysis, we introduce LATMiX, a method that enables affine transformations to be applied without runtime and memory overhead, fully comparable to leading approaches in this area. In our experiments, we showcase the effectiveness of LATMiX across seven benchmarks, as well as perplexity evaluation on WikiText2, achieving up to a 4% improvement in average accuracy recovery. Overall, our results indicate that learning affine transformations for MX formats in LLMs can yield substantial gains. While we did not evaluate LATMiX on non-MX data types in this work, its performance in such settings remains an interesting direction for future study. One limitation of LATMiX, shared with other optimization-based transformation methods, is the need for training; nevertheless, empirical results clearly demonstrate its benefits.

Impact Statement

This paper presents work whose goal is to advance the field of Machine Learning. There are many potential societal consequences of our work, none which we feel must be specifically highlighted here.

References

- AI, M. Meta LLaMA 3.2 models. Model card and documentation, 2024. Available at <https://github.com/meta-llama/llama-models> and <https://huggingface.co/meta-llama/Llama-3.2-3B>.
- Akhondzadeh, M. S., Bojchevski, A., Eleftheriou, E., and Dazzi, M. KurTail: Kurtosis-based LLM quantization. *arXiv preprint arXiv:2503.01483*, 2025.
- Alayrac, J.-B., Donahue, J., Luc, P., Miech, A., Barr, I., Hasson, Y., Lenc, K., Mensch, A., Millican, K., Reynolds, M., et al. Flamingo: a visual language model for few-shot learning. *Advances in neural information processing systems*, 35:23716–23736, 2022.
- Ashkboos, S., Croci, M. L., Nascimento, M. G. D., Hoefler, T., and Hensman, J. SliceGPT: Compress large language models by deleting rows and columns. In *The Twelfth International Conference on Learning Representations, ICLR 2024, Vienna, Austria, May 7-11, 2024*. OpenReview.net, 2024a.
- Ashkboos, S., Markov, I., Frantar, E., Zhong, T., Wang, X., Ren, J., Hoefler, T., and Alistarh, D. QUIK: Towards end-to-end 4-bit inference on generative large language models. In *Proceedings of the 2024 Conference on Empirical Methods in Natural Language Processing*, pp. 3355–3371, 2024b.
- Ashkboos, S., Mohtashami, A., Croci, M. L., Li, B., Cameron, P., Jaggi, M., Alistarh, D., Hoefler, T., and Hensman, J. QuaRot: Outlier-free 4-bit inference in rotated LLMs. *Advances in Neural Information Processing Systems*, 37:100213–100240, 2024c.
- Bisk, Y., Zellers, R., Gao, J., Choi, Y., et al. PIQA: Reasoning about physical commonsense in natural language. In *Proceedings of the AAAI conference on artificial intelligence*, volume 34, pp. 7432–7439, 2020.
- Bondarenko, Y., Nagel, M., and Blankevoort, T. Understanding and overcoming the challenges of efficient transformer quantization. In *Proceedings of the 2021 Conference on Empirical Methods in Natural Language Processing*, pp. 7947–7969, 2021.
- Brown, T., Mann, B., Ryder, N., Subbiah, M., Kaplan, J. D., Dhariwal, P., Neelakantan, A., Shyam, P., Sastry, G., Askell, A., et al. Language models are few-shot learners. *Advances in neural information processing systems*, 33: 1877–1901, 2020.
- Chee, J., Cai, Y., Kuleshov, V., and De Sa, C. M. QuIP: 2-bit quantization of large language models with guarantees. *Advances in Neural Information Processing Systems*, 36: 4396–4429, 2023.
- Chen, M. Evaluating large language models trained on code. *arXiv preprint arXiv:2107.03374*, 2021.
- Chmiel, B., Fishman, M., Banner, R., and Soudry, D. FP4 all the way: Fully quantized training of large language models. In *The Thirty-ninth Annual Conference on Neural Information Processing Systems*, 2025. URL <https://openreview.net/forum?id=kuzye4EPLR>.
- Clark, C., Lee, K., Chang, M.-W., Kwiatkowski, T., Collins, M., and Toutanova, K. BoolQ: Exploring the surprising difficulty of natural yes/no questions. *arXiv preprint arXiv:1905.10044*, 2019.
- Clark, P., Cowhey, I., Etzioni, O., Khot, T., Sabharwal, A., Schoenick, C., and Tafjord, O. Think you have solved question answering? try ARC, the AI2 reasoning challenge. *arXiv preprint arXiv:1803.05457*, 2018.
- Dettmers, T., Lewis, M., Belkada, Y., and Zettlemoyer, L. GPT3.int8(): 8-bit matrix multiplication for transformers at scale. *Advances in neural information processing systems*, 35:30318–30332, 2022.
- Dettmers, T., Svirschevski, R. A., Egiazarian, V., Kuznedelev, D., Frantar, E., Ashkboos, S., Borzunov, A., Hoefler, T., and Alistarh, D. SpQR: A sparse-quantized representation for near-lossless LLM weight compression. In *The Twelfth International Conference on Learning Representations, ICLR 2024, Vienna, Austria, May 7-11, 2024*. OpenReview.net, 2024.
- Dubey, A., Jauhri, A., Pandey, A., Kadian, A., Al-Dahle, A., Letman, A., Mathur, A., Schelten, A., Yang, A., Fan, A., et al. The llama 3 herd of models. *arXiv e-prints*, pp. arXiv–2407, 2024.
- Egiazarian, V., Castro, R. L., Kuznedelev, D., Panferov, A., Kurtic, E., Pandit, S., Marques, A., Kurtz, M., Ashkboos, S., Hoefler, T., et al. Bridging the gap between promise and performance for microscaling FP4 quantization. *arXiv preprint arXiv:2509.23202*, 2025.
- Frantar, E., Ashkboos, S., Hoefler, T., and Alistarh, D. OPTQ: accurate quantization for generative pre-trained transformers. In *The Eleventh International Conference on Learning Representations, ICLR 2023, Kigali, Rwanda, May 1-5, 2023*. OpenReview.net, 2023.

- Gao, L., Tow, J., Abbasi, B., Biderman, S., Black, S., DiPofi, A., Foster, C., Golding, L., Hsu, J., Le Noac’h, A., Li, H., McDonell, K., Muennighoff, N., Ociepa, C., Phang, J., Reynolds, L., Schoelkopf, H., Skowron, A., Sutawika, L., Tang, E., Thite, A., Wang, B., Wang, K., and Zou, A. The language model evaluation harness, 07 2024. URL <https://zenodo.org/records/12608602>.
- Gholami, A., Kim, S., Dong, Z., Yao, Z., Mahoney, M. W., and Keutzer, K. A survey of quantization methods for efficient neural network inference. In *Low-power computer vision*, pp. 291–326. Chapman and Hall/CRC, 2022.
- Gordon, O., Cohen, E., Habi, H. V., and Netzer, A. EPTQ: Enhanced post-training quantization via Hessian-guided network-wise optimization. In *European Conference on Computer Vision*, pp. 150–166. Springer, 2024.
- Hinton, G., Vinyals, O., and Dean, J. Distilling the knowledge in a neural network. *arXiv preprint arXiv:1503.02531*, 2015.
- Hoffmann, J., Borgeaud, S., Mensch, A., Buchatskaya, E., Cai, T., Rutherford, E., de Las Casas, D., Hendricks, L. A., Welbl, J., Clark, A., et al. Training compute-optimal large language models. In *Proceedings of the 36th International Conference on Neural Information Processing Systems*, pp. 30016–30030, 2022.
- Huang, L., Qin, J., Zhou, Y., Zhu, F., Liu, L., and Shao, L. Normalization techniques in training DNNs: Methodology, analysis and application. *IEEE transactions on pattern analysis and machine intelligence*, 45(8):10173–10196, 2023.
- Kaplan, J., McCandlish, S., Henighan, T., Brown, T. B., Chess, B., Child, R., Gray, S., Radford, A., Wu, J., and Amodei, D. Scaling laws for neural language models. *arXiv preprint arXiv:2001.08361*, 2020.
- Kim, S., Hooper, C. R. C., Gholami, A., Dong, Z., Li, X., Shen, S., Mahoney, M. W., and Keutzer, K. SqueezeLLM: Dense-and-sparse quantization. In *International Conference on Machine Learning*, pp. 23901–23923. PMLR, 2024.
- Kingma, D. P. and Ba, J. Adam: A method for stochastic optimization. In *Proceedings of the International Conference on Learning Representations ICLR 2015*, 2015.
- Kingma, D. P. and Dhariwal, P. Glow: Generative flow with invertible 1x1 convolutions. *Advances in neural information processing systems*, 31, 2018.
- Lee, J., Park, J., Cha, S., Cho, J., and Sim, J. MX+: Pushing the limits of microscaling formats for efficient large language model serving. In *Proceedings of the 58th IEEE/ACM International Symposium on Microarchitecture@*, pp. 869–883, 2025a.
- Lee, J., Park, J., Kim, J., Kim, Y., Oh, J., Oh, J., and Choi, J. AMXFP4: Taming activation outliers with asymmetric microscaling floating-point for 4-bit LLM inference. In *Findings of the Association for Computational Linguistics: ACL 2025*, pp. 14993–15013, 2025b.
- Lee, J. H., Kim, J., Kwon, S. J., and Lee, D. FlexRound: Learnable rounding based on element-wise division for post-training quantization. In *International Conference on Machine Learning*, pp. 18913–18939. PMLR, 2023.
- Li, G., Qiu, R., Chen, X., Ji, H., and Tong, H. Beyond log likelihood: Probability-based objectives for supervised fine-tuning across the model capability continuum. *arXiv preprint arXiv:2510.00526*, 2025.
- Li, J., Li, F., and Todorovic, S. Efficient Riemannian optimization on the Stiefel manifold via the Cayley transform. In *8th International Conference on Learning Representations, ICLR 2020, Addis Ababa, Ethiopia, April 26-30, 2020*. OpenReview.net, 2020.
- Lin, D., Talathi, S., and Annapureddy, S. Fixed point quantization of deep convolutional networks. In *International conference on machine learning*, pp. 2849–2858. PMLR, 2016.
- Lin, H., Xu, H., Wu, Y., Cui, J., Zhang, Y., Mou, L., Song, L., Sun, Z., and Wei, Y. DuQuant: Distributing outliers via dual transformation makes stronger quantized LLMs. *Advances in Neural Information Processing Systems*, 37: 87766–87800, 2024a.
- Lin, J., Tang, J., Tang, H., Yang, S., Chen, W.-M., Wang, W.-C., Xiao, G., Dang, X., Gan, C., and Han, S. AWQ: Activation-aware weight quantization for on-device LLM compression and acceleration. *Proceedings of machine learning and systems*, 6:87–100, 2024b.
- Liu, S.-Y., Liu, Z., Huang, X., Dong, P., and Cheng, K.-T. LLM-FP4: 4-bit floating-point quantized transformers. In *Proceedings of the 2023 Conference on Empirical Methods in Natural Language Processing*, pp. 592–605, 2023.
- Liu, Z., Zhao, C., Fedorov, I., Soran, B., Choudhary, D., Krishnamoorthi, R., Chandra, V., Tian, Y., and Blankevoort, T. SpinQuant: LLM quantization with learned rotations. In *The Thirteenth International Conference on Learning Representations, ICLR 2025, Singapore, April 24-28, 2025*. OpenReview.net, 2025.
- Loshchilov, I. and Hutter, F. Decoupled weight decay regularization. In *7th International Conference on Learning Representations, ICLR 2019, New Orleans, LA, USA, May 6-9, 2019*. OpenReview.net, 2019.

- Ma, Y., Li, H., Zheng, X., Ling, F., Xiao, X., Wang, R., Wen, S., Chao, F., and Ji, R. AffineQuant: Affine transformation quantization for large language models. In *The Twelfth International Conference on Learning Representations, ICLR 2024, Vienna, Austria, May 7-11, 2024*. OpenReview.net, 2024.
- Merity, S., Xiong, C., Bradbury, J., and Socher, R. Pointer sentinel mixture models. *arXiv preprint arXiv:1609.07843*, 2016.
- Mihaylov, T., Clark, P., Khot, T., and Sabharwal, A. Can a suit of armor conduct electricity? a new dataset for open book question answering. *arXiv preprint arXiv:1809.02789*, 2018.
- Nagel, M., Amjad, R. A., Van Baalen, M., Louizos, C., and Blankevoort, T. Up or down? adaptive rounding for post-training quantization. In *International conference on machine learning*, pp. 7197–7206. PMLR, 2020.
- Ramachandran, A., Kundu, S., and Krishna, T. MicroScopiQ: Accelerating foundational models through outlier-aware microscaling quantization. In *Proceedings of the 52nd Annual International Symposium on Computer Architecture*, pp. 1193–1209, 2025.
- Rouhani, B. D., Zhao, R., More, A., Hall, M., Khodamoradi, A., Deng, S., Choudhary, D., Cornea, M., Dellinger, E., Denolf, K., et al. Microscaling data formats for deep learning. *arXiv preprint arXiv:2310.10537*, 2023a.
- Rouhani, D. B., Garegrat, N., Savell, T., More, A., Han, K.-N., Zhao, R., Hall, M., Klar, J., Chung, E., Yu, Yuan Schulte, M., Wittig, Ralph Bratt, I., Stephens, N., Milanovic, J., Brothers, John Dubey, P., Cornea, M., Heinecke, A., Rodriguez, A., Langhammer, Martin Deng, S., Naumov, Maxim Micikevicius, P., and Siu, Michael Verrilli, C. OCP microscaling formats (MX) specification. Technical Report Version 1.0, Open Compute Project, Sep 2023b.
- Sakaguchi, K., Bras, R. L., Bhagavatula, C., and Choi, Y. WinoGrande: An adversarial winograd schema challenge at scale. *Communications of the ACM*, 64(9):99–106, 2021.
- Shao, W., Chen, M., Zhang, Z., Xu, P., Zhao, L., Li, Z., Zhang, K., Gao, P., Qiao, Y., and Luo, P. OmniQuant: Omnidirectionally calibrated quantization for large language models. In *The Twelfth International Conference on Learning Representations, ICLR 2024, Vienna, Austria, May 7-11, 2024*. OpenReview.net, 2024.
- Shao, Y., Wang, P., Chen, Y., Xu, C., Wei, Z., and Cheng, J. Block rotation is all you need for MXFP4 quantization. *arXiv preprint arXiv:2511.04214*, 2025.
- Sharify, S., Saxena, U., Xu, Z., Yazar, W., Soloveychik, I., and Wang, X. Post training quantization of large language models with microscaling formats. In *NeurIPS Efficient Natural Language and Speech Processing Workshop*, pp. 241–258. PMLR, 2024.
- Shen, S., Dong, Z., Ye, J., Ma, L., Yao, Z., Gholami, A., Mahoney, M. W., and Keutzer, K. Q-BERT: Hessian based ultra low precision quantization of BERT. In *Proceedings of the AAAI conference on artificial intelligence*, volume 34, pp. 8815–8821, 2020.
- Sun, Y., Liu, R., Bai, H., Bao, H., Zhao, K., Li, Y., Hu, J., Yu, X., Hou, L., Yuan, C., Jiang, X., Liu, W., and Yao, J. FlatQuant: Flatness matters for LLM quantization. In *Forty-second International Conference on Machine Learning, ICML 2025, Vancouver, BC, Canada, July 13-19, 2025*. OpenReview.net, 2025.
- Tseng, A., Chee, J., Sun, Q., Kuleshov, V., and De Sa, C. QuIP #: Even better LLM quantization with Hadamard incoherence and lattice codebooks. In *International Conference on Machine Learning*, pp. 48630–48656. PMLR, 2024.
- Vershynin, R. *High-dimensional probability: An introduction with applications in data science*, volume 47. Cambridge university press, 2018.
- Wei, J., Wang, X., Schuurmans, D., Bosma, M., Xia, F., Chi, E., Le, Q. V., Zhou, D., et al. Chain-of-thought prompting elicits reasoning in large language models. *Advances in neural information processing systems*, 35:24824–24837, 2022a.
- Wei, X., Zhang, Y., Zhang, X., Gong, R., Zhang, S., Zhang, Q., Yu, F., and Liu, X. Outlier suppression: Pushing the limit of low-bit transformer language models. *Advances in Neural Information Processing Systems*, 35:17402–17414, 2022b.
- Wei, X., Zhang, Y., Li, Y., Zhang, X., Gong, R., Guo, J., and Liu, X. Outlier suppression+: Accurate quantization of large language models by equivalent and effective shifting and scaling. In *Proceedings of the 2023 Conference on Empirical Methods in Natural Language Processing*, pp. 1648–1665, 2023.
- Xiao, G., Lin, J., Seznec, M., Wu, H., Demouth, J., and Han, S. SmoothQuant: Accurate and efficient post-training quantization for large language models. In *International conference on machine learning*, pp. 38087–38099. PMLR, 2023.
- Yang, A., Li, A., Yang, B., Zhang, B., Hui, B., et al. Qwen3 technical report. *arXiv preprint arXiv:2505.09388*, 2025.

- Yang, Z., Dai, Z., Yang, Y., Carbonell, J., Salakhutdinov, R. R., and Le, Q. V. Xlnet: Generalized autoregressive pretraining for language understanding. *Advances in neural information processing systems*, 32, 2019.
- Yao, Z., Yazdani Aminabadi, R., Zhang, M., Wu, X., Li, C., and He, Y. ZeroQuant: Efficient and affordable post-training quantization for large-scale transformers. *Advances in neural information processing systems*, 35: 27168–27183, 2022.
- Zellers, R., Holtzman, A., Bisk, Y., Farhadi, A., and Choi, Y. Hellaswag: Can a machine really finish your sentence? *arXiv preprint arXiv:1905.07830*, 2019.
- Zhao, W. X., Zhou, K., Li, J., Tang, T., Wang, X., Hou, Y., Min, Y., Zhang, B., Zhang, J., Dong, Z., et al. A survey of large language models. *arXiv preprint arXiv:2303.18223*, 2023.
- Zhao, Y., Lin, C.-Y., Zhu, K., Ye, Z., Chen, L., Zheng, S., Ceze, L., Krishnamurthy, A., Chen, T., and Kasikci, B. Atom: Low-bit quantization for efficient and accurate LLM serving. *Proceedings of Machine Learning and Systems*, 6:196–209, 2024.

A. MX Quantization Error Upper Bound (Theorem 3.3)

We split the proof of Theorem 3.3 into two parts. In the first part, we derive an upper bound without making any assumptions about the distribution of the feature map (i.e., the random vector \mathbf{x}). In the second part, we compute the expectation of the maximum absolute value of a sub-Gaussian vector and assume that \mathbf{x} follows a sub-Gaussian distribution to gain additional insight. We then combine these two parts to complete the proof.

The main assumption required for the proof is that the density of \mathbf{x} is bounded. More formally,

Assumption A.1. Assume that \mathbf{x} is a continuous random vector and that there exists a finite constant $C < \infty$ such that its probability density function $f(\mathbf{x})$ satisfies $0 \leq f(\mathbf{x}) < C \quad \forall \mathbf{x} \in \mathbb{R}^d$.

Lemma A.2. Assume that \mathbf{T} is an affine transformation and Q is MX quantization according to (1). Then,

$$\mathcal{E}(\mathbf{T}) \lesssim \frac{\|\mathbf{A}^{-1}\|_\sigma^2}{N_B} \sum_{i=1}^{N_B} \mathbb{E} \left[\left(\max_{j \in \mathcal{I}_i} |[\mathbf{T}(\mathbf{x})]_j| \right)^2 \right]. \quad (9)$$

Proof. We begin with the definition of quantization error in (2)

$$\begin{aligned} \mathcal{E}(\mathbf{T}) &\triangleq \frac{1}{d} \mathbb{E} \left[\left\| \mathbf{x} - \mathbf{T}^{-1} \left(Q \left(\mathbf{T}(\mathbf{x}) \right) \right) \right\|_2^2 \right] = \frac{1}{d} \mathbb{E} \left[\left\| \mathbf{A}^{-1} \left(\mathbf{T}(\mathbf{x}) - Q \left(\mathbf{T}(\mathbf{x}) \right) \right) \right\|_2^2 \right] \leq \frac{\|\mathbf{A}^{-1}\|_\sigma^2}{d} \mathbb{E} \left[\left\| \mathbf{T}(\mathbf{x}) - Q \left(\mathbf{T}(\mathbf{x}) \right) \right\|_2^2 \right] \\ &= \frac{\|\mathbf{A}^{-1}\|_\sigma^2}{N_B \cdot B} \mathbb{E} \left[\left\| \mathbf{y} - Q \left(\mathbf{y} \right) \right\|_2^2 \right] = \frac{\|\mathbf{A}^{-1}\|_\sigma^2}{N_B \cdot B} \sum_{i=1}^{N_B} \mathbb{E} \left[\left\| \mathbf{y}^{(i)} - Q \left(\mathbf{y}^{(i)} \right) \right\|_2^2 \right], \end{aligned} \quad (10)$$

where $\mathbf{y} = \mathbf{T}(\mathbf{x})$ is introduced for notational convenience and $\mathbf{y}^{(i)} = [\mathbf{y}_{i \cdot B} \quad \dots \quad \mathbf{y}_{(i+1) \cdot B - 1}]$ represents the vectorized features of the i^{th} MX-Block. In Eq. (2), the first equality follows from the invertibility of \mathbf{A} and the definition of the transformation:

$$\begin{aligned} \left\| \mathbf{x} - \mathbf{T}^{-1} \left(Q \left(\mathbf{T}(\mathbf{x}) \right) \right) \right\|_2^2 &= \left\| \mathbf{x} - \mathbf{A}^{-1} Q \left(\mathbf{T}(\mathbf{x}) \right) + \mathbf{A}^{-1} \mathbf{v} \right\|_2^2 = \left\| \mathbf{A}^{-1} \left(\mathbf{A} \mathbf{x} + \mathbf{v} - Q \left(\mathbf{T}(\mathbf{x}) \right) \right) \right\|_2^2 \\ &= \left\| \mathbf{A}^{-1} \left(\mathbf{T}(\mathbf{x}) - Q \left(\mathbf{T}(\mathbf{x}) \right) \right) \right\|_2^2. \end{aligned}$$

Next, we examine the error in each block and MX Quantization definition in (1):

$$\mathbb{E} \left[s_i^2 \left\| \frac{\mathbf{y}^{(i)}}{s_i} - Q_e \left(\frac{\mathbf{y}^{(i)}}{s_i} \right) \right\|_2^2 \right] = \mathbb{E} \left[s_i^2 \sum_{j=1}^B \left(\frac{\mathbf{y}_j^{(i)}}{s_i} - Q_e \left(\frac{\mathbf{y}_j^{(i)}}{s_i} \right) \right)^2 \right] = \mathbb{E} \left[s_i^2 \sum_{j=1}^B \mathbb{E} \left[\left(\frac{\mathbf{y}_j^{(i)}}{s_i} - Q_e \left(\frac{\mathbf{y}_j^{(i)}}{s_i} \right) \right)^2 \middle| s \right] \right]. \quad (11)$$

In Eq. (11), the first step splits the error by block, and the second applies the law of total expectation. We now derive the error for each element within a block.

$$\mathbb{E} \left[\left(\frac{\mathbf{y}_j^{(i)}}{s_i} - Q_e \left(\frac{\mathbf{y}_j^{(i)}}{s_i} \right) \right)^2 \middle| s \right] = \int_{\mathbf{y}_j^{(i)}} \left(\frac{\mathbf{y}_j^{(i)}}{s_i} - Q_e \left(\frac{\mathbf{y}_j^{(i)}}{s_i} \right) \right)^2 f_{\mathbf{y}_j^{(i)} | s_i} \left(\mathbf{y}_j^{(i)} | s_i \right) d\mathbf{y}_j^{(i)}. \quad (12)$$

Apply a change in variable $z = \frac{\mathbf{y}_j^{(i)}}{s_i}$, $d\mathbf{y}_j^{(i)} = s_i dz$ and combining with the definition of MX in (1) we assume that the domain of z is in the range of Q_e , results in

$$\begin{aligned} s_i \int_z (z - Q_e(z))^2 f_{\mathbf{y}_j^{(i)} | s_i}(z \cdot s_i | s_i) dz &= s_i \sum_{k=1}^{|\mathcal{Q}|} \int_{l_k}^{u_k} (z - q_k)^2 f_{\mathbf{y}_j^{(i)} | s_i}(z \cdot s_i | s_i) dz \\ &= \sum_{k=1}^{|\mathcal{Q}|} \int_{l_k}^{u_k} (z - q_k)^2 f_{z | s_i}(z | s_i) dz \leq C_Q \triangleq \sum_{k=1}^{|\mathcal{Q}|} \int_{l_k}^{u_k} (z - q_k)^2 dz. \end{aligned} \quad (13)$$

Where, q_k is the quantized value in the interval between l_k to u_k and in the last step in Eq. (13) we upper bound the probability over the interval between u_k to l_k as we assume that the probability density can be bounded by some constant. Combining Eq.(13), (12), (11) and (10) results in:

$$\begin{aligned} \mathcal{E}(\mathbf{T}) &\leq \left\| \mathbf{A}^{-1} \right\|_{\sigma}^2 C_Q \frac{1}{N_B} \sum_{i=1}^{N_B} \mathbb{E} \left[s_i^2 \right] = \left\| \mathbf{A}^{-1} \right\|_{\sigma}^2 C_Q \frac{1}{N_B} \sum_{i=1}^{N_B} \mathbb{E} \left[2 \left\lceil \log_2 \left(\max_{j \in \mathcal{I}_i} |\mathbf{y}_j| \right) \right\rceil^{-2r_{max}} \right] \\ &\leq \left\| \mathbf{A}^{-1} \right\|_{\sigma}^2 C_Q \frac{2^{-2r_{max}}}{N_B} \sum_{i=1}^{N_B} \mathbb{E} \left[\left(\max_{j \in \mathcal{I}_i} |\mathbf{y}_j| \right)^2 \right]. \end{aligned} \quad (14)$$

In (14), the first equality follows from the definition of MX quantization in (1), and the second inequality follows from the definition of the floor function. \square

Lemma A.2 establishes the first part of Theorem 3.3, namely inequality (3). To prove the second part of Theorem 3.3, we now present and prove an upper bound on the expected maximum of a sub-Gaussian vector.

Lemma A.3. *Let $\mathbf{y} \in \mathbb{R}^B$ be a random vector with mean $\boldsymbol{\mu}$, $\|X\|_{\psi_2}$ is sub-Gaussian norm of random variable X . Assume that \mathbf{y} is a sub-Gaussian random vector. Then,*

$$\mathbb{E} \left[\left(\max_j |\mathbf{y}_j| \right)^p \right]^{1/p} \leq \max_j |\boldsymbol{\mu}_j| + \frac{\max_i \|\mathbf{y} - \boldsymbol{\mu}\|_{\psi_2}}{\sqrt{c}} \left((\log(2B))^{p/2} + B \cdot p \cdot \Gamma(p/2, \log(2B)) \right)^{1/p} \quad (15)$$

Proof. We start by centering \mathbf{y} and placing an upper bound on its absolute maximum.

$$\max_j |\mathbf{y}_j| = \max_j |\mathbf{y} - \boldsymbol{\mu} + \boldsymbol{\mu}_j| \leq \max_j |\mathbf{y} - \boldsymbol{\mu}_j| + \max_j |\boldsymbol{\mu}_j| \quad (16)$$

Next, by definition of the L_p norm of a random variable, we obtain:

$$\mathbb{E} \left[\left(\max_j |\mathbf{y}_j| \right)^p \right]^{1/p} = \left\| \max_j |\mathbf{y}_j| \right\|_{L_p} = \left\| \max_j |\mathbf{y} - \boldsymbol{\mu}_j| + \max_j |\boldsymbol{\mu}_j| \right\|_{L_p} \leq \max_j |\boldsymbol{\mu}_j| + \left\| \max_j |\mathbf{y} - \boldsymbol{\mu}_j| \right\|_{L_p}. \quad (17)$$

In Eq. (17), the first step follows from the definition of the random-variable L_p norm (see (Vershynin, 2018), Chapter 1.3); the second uses the triangle inequality, and the last uses that $\boldsymbol{\mu}$ is deterministic (i.e., not a random variable). For notational convenience, let us denote $z = \max_j |\mathbf{y} - \boldsymbol{\mu}_j|$. We then only need to evaluate the second term in (17):

$$\left\| \max_j |\mathbf{y} - \boldsymbol{\mu}_j| \right\|_{L_p} = \mathbb{E} [z^p]^{1/p}. \quad (18)$$

To compute $\mathbb{E} [z^p]$ we first compute the tail bound of z .

$$\mathbb{P}(z \geq t) = \mathbb{P} \left(\bigcup_i |\mathbf{y} - \boldsymbol{\mu}_i| \geq t \right) \leq \sum_i \mathbb{P} \left(|\mathbf{y} - \boldsymbol{\mu}_i| \geq t \right) \leq 2 \cdot B \cdot \exp \left(-c \frac{t^2}{K^2} \right), \quad (19)$$

where c is an absolute constant. In Eq. (19), the first equality is valid by definition, the second follows from the union bound, and the last uses the fact that $|\mathbf{y} - \boldsymbol{\mu}_i|$ is sub-Gaussian with maximal sub-Gaussian norm from all the variables is bounded by: $K \triangleq \max_i \|\mathbf{y} - \boldsymbol{\mu}_i\|_{\psi_2}$ combine with the tails probability of sub-Gaussian r.v ((Vershynin, 2018) Proposition 2.6.6).

$$\begin{aligned} \mathbb{E} [z^p] &= \int_0^{\infty} p t^{p-1} \mathbb{P}(z \geq t) dt = \int_0^{t_0} p t^{p-1} \mathbb{P}(z \geq t) dt + \int_{t_0}^{\infty} p t^{p-1} \mathbb{P}(z \geq t) dt \\ &\leq \int_0^{t_0} p t^{p-1} dt + \int_{t_0}^{\infty} p t^{p-1} \mathbb{P}(z \geq t) dt \end{aligned} \quad (20)$$

By selection $t_0 = K\sqrt{\frac{1}{c} \log(2B)}$ we have:

$$\int_0^{t_0} pt^{p-1} dt = t_0^p = K^p \left(\frac{1}{c} \log(2B) \right)^{p/2}. \quad (21)$$

and,

$$\begin{aligned} \int_{t_0}^{\infty} pt^{p-1} \mathbf{P}(z \geq t) dt &\leq 2dp \int_{t_0}^{\infty} t^{p-1} \exp\left(-c \frac{t^2}{K^2}\right) dt = B \cdot p \left(\frac{K}{\sqrt{c}}\right)^p \int_{\log(2B)}^{\infty} u^{p/2-1} \exp(-u) du \\ &= B \cdot p \left(\frac{K}{\sqrt{c}}\right)^p \Gamma(p/2, \log(2B)) \end{aligned} \quad (22)$$

In Eq. (22), the first inequality follows from Eq. (19), the second step applies the change of variables $u = ct^2/K^2$, which implies $t = \frac{K\sqrt{u}}{\sqrt{c}}$ and $dt = \frac{K}{2\sqrt{c}} u^{-0.5} du$. The third step uses the definition of the incomplete Gamma function. Combining Eq. (21) and Eq. (22) into Eq. (20) results in:

$$\left\| \max_j [\mathbf{y} - \boldsymbol{\mu}]_j \right\|_{L_p} = \mathbb{E}[z^p]^{1/p} \leq \frac{K}{\sqrt{c}} \left((\log(2B))^{p/2} + B \cdot p \cdot \Gamma(p/2, \log(2B)) \right)^{1/p}. \quad (23)$$

Finally, combining Eq. (23) with Eq. (17) yields the desired results. \square

Defining $\mathbf{y} = \mathbf{T}(\mathbf{x})$, it follows that $\boldsymbol{\mu}_y = \mathbb{E}[\mathbf{y}] = \mathbf{T}(\mathbb{E}[\mathbf{x}]) = \mathbf{T}(\boldsymbol{\mu})$. Applying Lemma A.3 with $p = 2$, we obtain

$$M_i \triangleq \mathbb{E} \left[\left(\max_{j \in \mathcal{I}_i} |[\mathbf{T}(\mathbf{x})]_j| \right)^2 \right] \leq \left(\max_{j \in \mathcal{I}_i} |[\boldsymbol{\mu}_y]_j| + \frac{\max_{j \in \mathcal{I}_i} \|[\mathbf{T}(\mathbf{x}) - \mathbf{T}(\boldsymbol{\mu})]_j\|_{\psi_2}}{\sqrt{c}} (1 + \log(2B))^{1/2} \right)^2. \quad (24)$$

Note that incomplete Gamma of $\Gamma(1, x) = \exp(-x)$ which in our case results in $\Gamma(1, \log(2B)) = \frac{1}{2B}$.

B. Affine Transformation inside MHA

Here, we show that affine transformation can be incorporated into MHA in the general case, and then we detail the corresponding folding operation. Concretely, let $\mathbf{X} \in \mathbb{R}^{N_T \times d}$ denote the input to the MHA, $\mathbf{P}_h \in \mathbb{R}^{N_T \times N_T}$ the attention matrix of the h^{th} head, $\mathbf{W}_V^{(h)}$ the value projection matrix of the h^{th} head, \mathbf{W}_O the output projection matrix and N_T is the number of tokens. Since the transformation is applied independently to each token, we define the transformation over multiple tokens as follows:

$$\mathbf{T}_2(\mathbf{X}) = \mathbf{X}\mathbf{A}_2 + \mathbf{V}_2 \quad (25)$$

and its inverse

$$\mathbf{T}_2^{-1}(\mathbf{X}) = \mathbf{X}\mathbf{A}_2^{-1} - \mathbf{V}_2\mathbf{A}_2^{-1} \quad (26)$$

where $\mathbf{V}_2 \in \mathbb{R}^{N_T \times d}$ denotes the shift matrix, in which the shift vector is replicated across all tokens. Now, we apply it to the multi-head attention block:

$$\mathbf{Y} = \text{Cat} \left(\left[\mathbf{P}_1 \mathbf{T}_2(\mathbf{X}\mathbf{W}_V^{(1)}), \dots, \mathbf{P}_H \mathbf{T}_2(\mathbf{X}\mathbf{W}_V^{(H)}) \right] \right) \quad (27)$$

Next, we apply the inverse transformation to \mathbf{Y} and then perform the output projection, yielding $\mathbf{G}^{-1}(\mathbf{Y})\mathbf{W}_O$. Because this transformation operates independently on each token, we can, without loss of generality, analyze a single head:

$$\begin{aligned} \mathbf{T}_2^{-1} \left(\mathbf{P}_1 \mathbf{T}_2(\mathbf{X}\mathbf{W}_V^{(1)}) \right) &= \mathbf{P}_1 \mathbf{T}_2(\mathbf{X}\mathbf{W}_V^{(1)}) \mathbf{A}_2^{-1} - \mathbf{V}_2 \mathbf{A}_2^{-1} = \mathbf{P}_1 \mathbf{X} \mathbf{W}_V^{(1)} \mathbf{A}_2 \mathbf{A}_2^{-1} + \mathbf{P}_1 \mathbf{V}_2 \mathbf{A}_2^{-1} - \mathbf{V}_2 \mathbf{A}_2^{-1} \\ &= \mathbf{P}_1 \mathbf{X} \mathbf{W}_V^{(1)} \end{aligned} \quad (28)$$

In the final step of (28), we exploit that \mathbf{P} arises from a softmax and that \mathbf{V}_2 is replicated across tokens, which implies: $\mathbf{P}_1 \mathbf{V}_2 \mathbf{A}_2^{-1} = \mathbf{V}_2 \mathbf{A}_2^{-1}$. In this way, we can add an affine transformation to the MHA block.

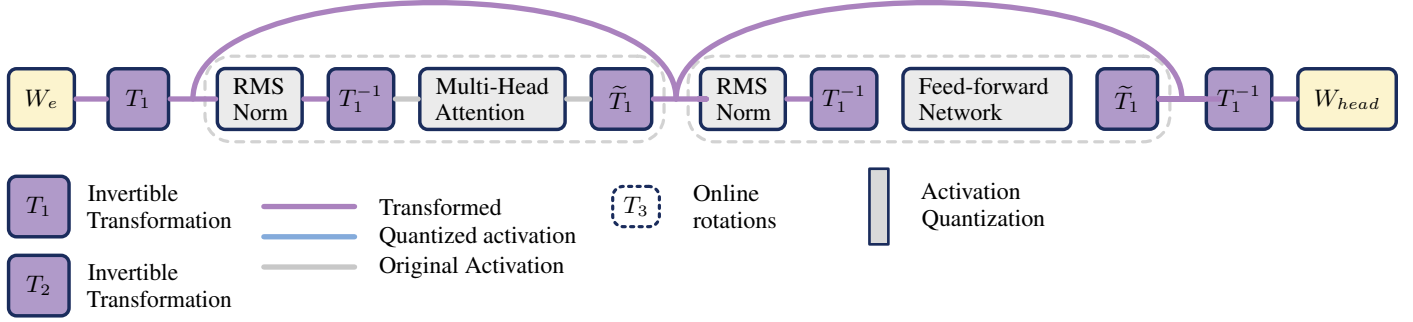
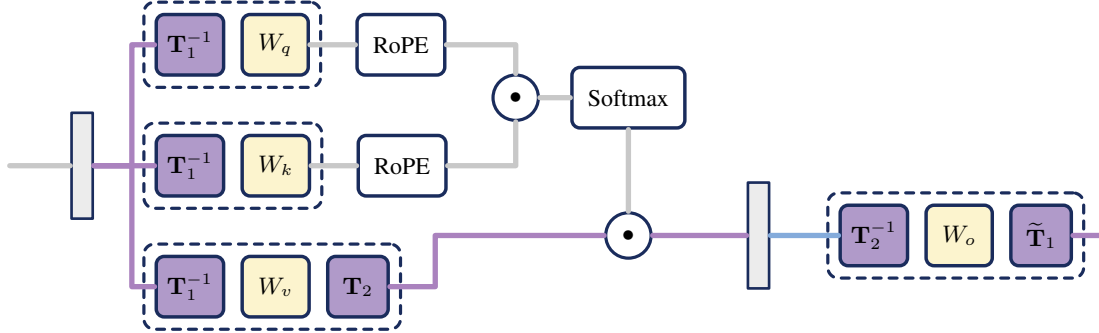
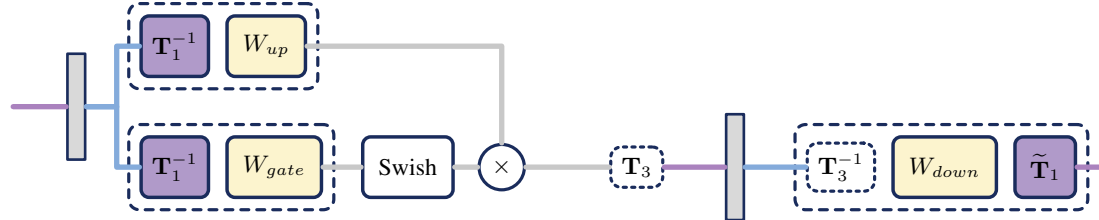

 (a) Location of \mathbf{T}_1 transformation of LLM that enables the folding of general invertible transformation.

 (b) Location of \mathbf{T}_1 transformation of LLM that enables the folding of general invertible transformation.

 (c) Location of \mathbf{T}_1 and \mathbf{T}_3 transformation of LLM with inside view of Feed-Forward Block.

Figure 4. Location of all transformations on a regular LLM with marking of folding operations.

C. Folding & Transformation Structure

We adopt the same transformation locations as in (Liu et al., 2025) and adapt them to the micro-scaling setup of (Egiazarian et al., 2025). First, we fold the RMS-Norm parameter into the following linear layer as in (Ashkboos et al., 2024c). Concretely, we apply three transformations at the same places as in (Egiazarian et al., 2025): (i) \mathbf{T}_1 , a transformation applied to the residual path of the model; (ii) \mathbf{T}_2 , a transformation applied to the value vectors in multi-head attention; and (iii) \mathbf{T}_3 (shown in in Fig. 4c), an *online* block Hadamard transformation as in (Egiazarian et al., 2025). Now, we describe the folding of the transformations \mathbf{T}_1 and \mathbf{T}_2 such that those transformations will add zero cost to the inference runtime and model size as they are folded to the exiting operation. As shown in LATMiX, we derived a way to learn an affine transformation in an LLM so that it can be absorbed into the adjacent linear operation. This eliminates the need to explicitly handle the RMSNorm (e.g. using orthogonal transformation), since it is already taken into account during the optimization process.

C.1. Folding of \mathbf{T}_1

To fold \mathbf{T}_1 we need to take into account the shift v_1 and the matrix \mathbf{A}_1 due to the residual structure of LLM (see Fig. 4), we only add the shift vector v_1 once after the embedding layer and remove every block using the inverse transformation. The matrix \mathbf{A}_1 is applied to the output of each block, and we define this transformation as $\tilde{\mathbf{T}}_1(x) = \mathbf{A}_1 x$. Next, we describe how to fold the \mathbf{T}_1 :

- **Folding \mathbf{T}_1^{-1} :** \mathbf{T}_1^{-1} is folded into the K, Q, and V linear mappings within the multi-head attention block. Denote the linear operator for the K, Q, and V features by $f_\Gamma(\mathbf{x}) = \mathbf{W}_\Gamma \mathbf{x} + \mathbf{b}_\Gamma$, where $\Gamma \in \{K, Q, V\}$. After applying this transformation, we introduce \tilde{f}_X to represent the resulting folded operation:

$$\begin{aligned} \tilde{f}_\Gamma(\mathbf{x}) &\triangleq f_\Gamma(\mathbf{T}_1^{-1}(\mathbf{x})) = \mathbf{W}_\Gamma \mathbf{T}_1^{-1}(\mathbf{x}) + \mathbf{b}_\Gamma = \mathbf{W}_\Gamma (\mathbf{A}_1^{-1} \mathbf{x} - \mathbf{A}_1^{-1} \mathbf{v}_1) + \mathbf{b}_\Gamma \\ &= \underbrace{\mathbf{W}_\Gamma \mathbf{A}_1^{-1}}_{=\tilde{\mathbf{W}}_\Gamma} \mathbf{x} + \underbrace{\mathbf{b}_\Gamma - \mathbf{W}_\Gamma \mathbf{A}_1^{-1} \mathbf{v}_1}_{=\tilde{\mathbf{b}}_\Gamma}. \end{aligned} \quad (29)$$

From (29), it follows that \tilde{f}_Γ can be represented as a linear operator with a weight matrix $\tilde{\mathbf{W}}_\Gamma$ and a bias vector $\tilde{\mathbf{b}}_\Gamma$.

- **Folding $\tilde{\mathbf{T}}_1$:** The transformation $\tilde{\mathbf{T}}_1$ can be folded into the linear output operation of the Feed-Forward block and the projection set in the MHA. Specifically, let $f_O(\mathbf{x}) = \mathbf{W}_O \mathbf{x} + \mathbf{b}_O$ be the linear output operation of the FFN and MHA. Applying the transformation to the output of the linear operation yields the following.

$$\tilde{f}_O(\mathbf{x}) = \tilde{\mathbf{T}}_1(f_O(\mathbf{x})) = \mathbf{A}_1 f_O(\mathbf{x}) = \underbrace{\mathbf{A}_1 \mathbf{W}_O}_{=\tilde{\mathbf{W}}_O} \mathbf{x} + \underbrace{\mathbf{A}_1 \mathbf{b}_O}_{=\tilde{\mathbf{b}}_O}. \quad (30)$$

From (30), it follows that \tilde{f}_O can be represented as a linear operator with a weight matrix $\tilde{\mathbf{W}}_O$ and a bias vector $\tilde{\mathbf{b}}_O$.

- **Folding \mathbf{T}_1 :** \mathbf{T}_1 is applied only to the embedding matrix. Specifically, let \mathbf{W}_e denote the embedding matrix and \mathbf{w}_j the j^{th} embedding vector. We apply the transformation to the feature after the embedding step, which is equivalent to applying the transformation to each embedding vector individually, resulting in:

$$\tilde{\mathbf{w}}_j = \mathbf{T}_1(\mathbf{w}_j) = \mathbf{A}_1 \mathbf{w}_j + \mathbf{v}_1. \quad (31)$$

This means that $\tilde{\mathbf{w}}_j$ represents the folded embedding vectors.

C.2. Folding of \mathbf{T}_2

After folding the transformation \mathbf{T}_1 we describe here the folding of \mathbf{T}_2 into V linear operation and output linear transformation of the Multi-head attention block. Note that there is a separate transformation \mathbf{T}_2 for each Multi-Head Attention Block.

Now we fold \mathbf{T}_2 into the linear operation V and inverse the operation in the MHA output project.

- **Fold \mathbf{T}_2 into Values linear projection** Since \mathbf{T}_1^{-1} has already been absorbed into the linear projection of Values as shown in (29), we now add to it \mathbf{T}_2 , which we denote by \tilde{f} and compute as follows:

$$\tilde{f}(\mathbf{x}) \triangleq \mathbf{T}_2(\tilde{f}_V(\mathbf{x})) = \mathbf{A}_2 \tilde{f}_V(\mathbf{x}) + \mathbf{v}_2 = \underbrace{\mathbf{A}_2 \mathbf{W}_V \mathbf{A}_1^{-1}}_{=\tilde{\mathbf{W}}_V} \mathbf{x} + \underbrace{\mathbf{A}_2 \mathbf{b}_V - \mathbf{A}_2 \mathbf{W}_V \mathbf{A}_1^{-1} \mathbf{v}_1 + \mathbf{v}_2}_{=\tilde{\mathbf{b}}_V} \quad (32)$$

Finally, the linear operation of V has the weights matrix $\tilde{\mathbf{W}}_V$ and the bias vector $\tilde{\mathbf{b}}_V$.

- **Fold \mathbf{T}_2^{-1} into the output Projection** Analogous to the folding into V, we have incorporated the transformation \mathbf{T}_1 into the output projection matrix, as indicated in (30). We now add to it \mathbf{T}_2^{-1} , which yields $\tilde{f}_O(\mathbf{x})$ and is given by:

$$\tilde{f}_O(\mathbf{x}) = \tilde{f}_O(\mathbf{T}_2^{-1}(\mathbf{x})) = \underbrace{\mathbf{A}_1 \mathbf{W}_O}_{=\tilde{\mathbf{W}}_O} \mathbf{T}_2^{-1}(\mathbf{x}) + \underbrace{\mathbf{A}_1 \mathbf{b}_O}_{=\tilde{\mathbf{b}}_O} = \underbrace{\mathbf{A}_1 \mathbf{W}_O \mathbf{A}_2^{-1}}_{=\tilde{\mathbf{W}}_O} \mathbf{x} - \underbrace{\mathbf{A}_1 \mathbf{W}_O \mathbf{A}_2^{-1} \mathbf{v}_2 + \mathbf{A}_1 \mathbf{b}_O}_{=\tilde{\mathbf{b}}_O} \quad (33)$$

Finally, the linear operation of the MHA output projections has the weights matrix $\tilde{\mathbf{W}}_O$ and the bias vector $\tilde{\mathbf{b}}_O$.

D. Implementation Details

The implementation of our algorithm, as well as all evaluated reference methods, is built on top of the microscaling quantization and GPTQ codebase provided by [Egiazarian et al. \(2025\)](#).

The transformations T_1 and T_2 are applied in the same manner as R_1 and R_2 in [Liu et al. \(2025\)](#) and [Ashkboos et al. \(2024c\)](#). The exact mechanism is described in Section 3 of the main paper. All compared reference methods are evaluated using the same transformation structure. In addition, an online Hadamard transformation is applied to the *down* linear operator in the MLP component of each transformer block, following the setup of the cited works. This transformation is not part of the LATMiX algorithm and is included solely to ensure a fair and consistent comparison.

All experiments were conducted on a single NVIDIA A100 GPU. For calibration, we used 256 randomly sampled sequences from the WikiText2 dataset ([Merity et al., 2016](#)), each with a sequence length of 1,024. The same calibration set is used both for transformation training and for the GPTQ procedure.

Transformation training is performed using the AdamW optimizer ([Loshchilov & Hutter, 2019](#)) with weight-decay, together with a cosine learning-rate scheduler and a linear warmup with start and end factors of 0.1 and 1, respectively. We run 1,000 training steps for the LU parametrization and 2,500 steps for the QR parametrization. The transformation matrix is initialized in a block-diagonal fashion, with small Gaussian noise added to the off-diagonal entries. Each block is a 32×32 matrix, initialized as a random Hadamard matrix for the LU parametrization or as a random orthogonal matrix for the QR parametrization.

D.1. Training Hyperparameters

We used the largest batch size permitted by GPU memory for each model, ranging from 1 for the largest models to 8 for smaller ones. The learning rate was tuned separately for each model to ensure stable and effective optimization, with values selected from the range 10^{-4} to 10^{-5} .

In addition, we incorporate two mechanisms into the training procedure to improve stability and perform a sweep to tune their hyperparameters. The first is a regularization term applied to the diagonal entries of the learned transformation matrix, encouraging them to remain close to one. This prevents the diagonal from growing or shrinking excessively, which could otherwise lead to unstable training behavior.

We observe that this regularization has a relatively small but consistent effect. While it does not substantially change the final performance, it helps guide training toward a more stable and better-performing solution. We hypothesize that this limited impact is due to the initialization of the transformation as an orthogonal matrix, whose diagonal entries are already close to one and thus near a good operating point.

In addition, following common practice in knowledge-distillation-based methods ([Hinton et al., 2015](#); [Huang et al., 2023](#)), we introduce a temperature parameter in the distillation loss. Similar to the diagonal regularization, we do not observe a strong sensitivity to the temperature value. However, in several cases it helps the optimization converge to a slightly improved solution.

D.2. Evaluated references Setting

As mentioned earlier, we evaluate a range of existing methods for LLM quantization. Achieving a fair comparison poses significant challenges, as many of these methods were not originally designed for MX quantization, and were evaluated under different quantization formats, transformation choices, and implementation settings. To address this, we re-implement most methods within the same experimental setup and codebase used to evaluate LATMiX, ensuring consistency across comparisons.

It is important to note that some methods required modifications that deviate from their exact original configurations. In particular, for FlatQuant ([Sun et al., 2025](#)), we define the learnable matrix A_1 as a global transformation, rather than a per-block transformation as proposed in the original paper. In addition, we evaluate FlatQuant using both the original loss defined in their work, which is computed per block, and our distillation-based loss (see Section 8). The results reported in Section 5 correspond to the runs using our loss, which consistently outperform those obtained with the original FlatQuant loss. One additional deviation from the SpinQuant setup is the omission of the online Hadamard rotation they apply to the RoPE output, following the setup set by ([Egiazarian et al., 2025](#)).

E. Additional Experiments

E.1. Perplexity Results

Table 3. Perplexity Comparison on WikiText2 for different quantization methods under MXFP4 quantization for both weights and activations. Best results are highlighted in bold, and second best in underline.

Method	Llama3.2-1B	Llama3.2-3B	Llama3-8B	Qwen2.5-1.5B	Qwen2.5-3B	Qwen3-1.7B	Qwen3-4B	Qwen3-8B
FP16	9.75	7.81	6.14	9.27	8.02	16.71	13.66	9.72
RTN	17.01	10.42	8.22	15.26	12.18	22.37	16.78	11.29
QuaRot-RTN	19.00	12.41	11.24	14.58	11.28	51.74	19.94	13.55
GPTQ	18.80	45.69	7.97	13.53	10.86	21.29	15.82	10.90
QuaRot	12.87	9.56	8.10	11.63	9.62	20.24	19.21	10.99
SpinQuant	12.74	8.93	7.44	11.39	11.35	19.21	<u>13.53</u>	10.19
FlatQuant	12.79	9.66	7.81	11.53	9.60	19.28	15.10	11.02
BRQ	11.93	9.08	7.13	11.95	9.46	–	–	–
MR-GPTQ	12.36	9.03	<u>7.11</u>	11.49	9.64	21.30	16.17	10.59
LATMiX-LU (Ours)	11.69	8.70	7.08	10.95	9.12	16.98	13.85	<u>10.13</u>
LATMiX-QR (Ours)	<u>11.82</u>	<u>8.75</u>	7.12	<u>11.02</u>	<u>9.19</u>	16.88	13.39	9.89

We evaluate quantization performance on the WikiText2 language modeling benchmark (Merity et al., 2016), a standard dataset of high-quality Wikipedia articles evaluated using perplexity. In the table, BRQ results refer to learned block-wise rotation transformation taken from (Shao et al., 2025). As this study did not present results in Qwen3-1.7B, Qwen3-4B, and Qwen3-8B, we left the corresponding cells empty. All other results were obtained using MR-GPTQ (Egiazarian et al., 2025) publicly released codebase, with adaptations following SpinQuant’s (Liu et al., 2025) transformation setting. QuaRot refers to our implementation of tensor-wise Hadamard rotation following (Ashkboos et al., 2024c). The results are presented in Table 3. Consistent with the trends observed in Section 5 across other language benchmarks, this experiment shows that learning a general affine transformation is more effective than relying on standard rotation-based approaches.

In addition, we examine how these results change when learning is restricted to orthogonal matrix transformations, as in BRQ (Shao et al., 2025). Following the comparison in Table 3, we find that limiting the transformation to be strictly orthogonal is insufficient and leads to suboptimal performance across models. In contrast, allowing a general invertible transformation provides additional flexibility, enabling more effective redistribution of the activation tensor energy beyond what is achievable with orthogonal rotations alone.

E.2. Initialization of the Transformations

Table 4. Ablation study on the different methods for initializing the learned transformation matrix, evaluated on WikiText2 perplexity.

Initialization Method	Llama3.2-1B		Qwen3-1.7B	
	LU	QR	LU	QR
Identity	12.23	12.12	17.81	17.11
Identity + Noise	12.25	12.11	18.17	17.91
Full Orthogonal	11.86	12.35	17.73	17.64
BD Orthogonal	12.04	11.87	17.34	17.90
BD Orthogonal + Noise	12.07	11.82	17.08	16.88
Full Hadamard	12.27	12.14	17.47	18.01
BD Hadamard	11.71	12.13	17.18	18.35
BD Hadamard + Noise	11.69	12.09	16.98	18.12

We examined several strategies for initializing the learned transformation matrices. Specifically, we considered initialization as the **Identity** matrix, a random **Orthogonal** matrix, or a random **Hadamard** matrix. For the latter two, we additionally evaluated block-diagonal (**BD**) variants of the initialization. For all diagonal or block-diagonal initializations, we further considered adding small random Gaussian noise to the off-diagonal or off-block-diagonal entries, with the aim of improving optimization stability during training.

The results reported in Table 4 indicate that block-diagonal initialization with small random noise consistently outperforms the other initialization strategies. This behavior aligns with the intuition that a block-diagonal structure is well matched to the MX quantization regime, as it encourages more uniform redistribution of outliers within each quantization block during

the early stages of training. As observed in other ablations in Section 5, the optimization subsequently departs from the initial block-orthogonal structure, enabling controlled transfer of activation energy across blocks and converging to a more effective solution.

E.3. Loss Function for LATMiX

Here, we justify the choice of the Kullback–Leibler divergence as a measure of the discrepancy between the floating-point and quantized modes. Specifically, let \mathbf{X} denote an input context to the model and let Y be a random matrix representing the expected response; we use the expected negative log-likelihood (NLL) as a measure of the model performance (Yang et al., 2019; Li et al., 2025):

$$\mathcal{L}(P_\theta) \triangleq \mathbb{E}_{Y, \mathbf{X}} \left[-\log \left(P_\theta(Y|\mathbf{X}) \right) \right] = \mathbb{E}_{\mathbf{X}} \left[\mathbb{E}_{Y \sim Q(\cdot|\mathbf{X})} \left[-\log \left(P_\theta(Y|\mathbf{X}) \right) \right] \right], \tag{34}$$

where $P_\theta(Y|\mathbf{X})$ represents the probability that the LLM f assigns to each output token (typically computed via a softmax layer), and Q denotes the probability distribution over all possible responses given the context \mathbf{X} . Let \tilde{P}_Φ be the quantized model, parameterized by $\Phi = \{\theta, \Omega\}$, where θ are the original model parameters and Ω are the transformation parameters. We analyze the difference between the NLL of the quantized model and that of the full-precision (floating-point) model.

Proposition E.1. *Let $\epsilon > 0$ denote a lower bound on the probability values. Suppose that $\epsilon \leq P_\theta(Y|\mathbf{X}) \quad \forall Y, \mathbf{X}$, and $\epsilon \leq \tilde{P}_\Phi(Y|\mathbf{X}) \quad \forall Y, \mathbf{X}$. Then,*

$$\min_{\Omega} \Delta(\Omega) \triangleq \min_{\Omega} \left| \mathcal{L}(\tilde{P}_\Phi) - \mathcal{L}(P_\theta) \right| \leq C + \min_{\Omega} \mathbb{E}_{\mathbf{X}} \left[\text{KL} \left(P_\theta(Y|\mathbf{X}), \tilde{P}_\Phi(Y|\mathbf{X}) \right) \right], \tag{35}$$

where C is constant independent of Ω .

The proof is described in Appendix E.3.1. From Proposition E.1, we observe that the mismatch between the quantized model and its floating-point counterpart is captured by an upper bound based on the expected KL divergence over all possible contexts. This establishes a connection between the KL loss and the NLL loss of the downstream task. In practice, however, we typically lack direct access to samples of the downstream task. Yet, it is common to assume access to a corpora of texts and solve a language modeling task instead. Under this assumption, the bound reduces to that in Eq. (8), which is simply the KL divergence between the quantized model and the floating-point model.

Moreover, we investigated three numerical loss functions that are widely used in previous work: (i) MSE applied to the output of each transformer block (Sun et al., 2025) between the quantized and floating-point representations; (ii) cross-entropy loss for the prediction of the next-token (Liu et al., 2025); and (iii) KL divergence between the predictions of the quantized and the floating-point networks. Specifically, we trained an affine transformation with all three losses on Llama3.2-1B and Qwen3-1.7B while quantizing to MXFP4. We report both perplexity on WikiText2 and the average accuracy on the following zero-shot tasks: RC Easy, WinoGrande, PIQA, BoolQ, and OpenBookQA. For all benchmarks, the transformations are learned using WikiText2, making evaluations on WikiText2 in-distribution and zero-shot task evaluations out-of-distribution.

From Table 5, we see that the KL loss outperforms the other loss functions in terms of average accuracy on zero-shot tasks. In addition, while it surpasses the MSE loss in terms of WikiText2 perplexity, it yields a higher perplexity compared to the CE loss. This suggests that using CE loss fits better when learning the transformations on the same dataset and task, but worse in zero-shot tasks.

Table 5. Ablation study comparing WikiText2 perplexity (\downarrow) and zero-shot average accuracy (Avg. Acc. \uparrow) for mean squared error (MSE) loss, KL divergence on model predictions, and cross-entropy loss based on next token predictions.

Loss Function	Llama3.2-1B		Qwen3-1.7B	
	Wiki	Avg. Acc.	Wiki	Avg. Acc.
FP16	9.75	60.02	16.71	63.39
MSE	12.18	55.09	20.86	59.72
CE	11.27	56.19	13.42	58.87
KL	11.69	56.32	16.98	60.48

E.3.1. PROOF PROPOSITION E.1

Proof. First, we apply the definition of the NNL loss given in (34)

$$\left| \mathcal{L}(\tilde{P}_\Phi) - \mathcal{L}(P_\theta) \right| = \left| \mathbb{E}_{\mathbf{X}} \left[\mathbb{E}_{Y \sim Q(\cdot|\mathbf{X})} \left[-\log \left(\frac{\tilde{P}_\Phi(Y|\mathbf{X})}{P_\theta(Y|\mathbf{X})} \right) \right] \right] \right|. \quad (36)$$

Next, we insert and subtract the floating-point model probability $P_\theta(Y|\mathbf{X})$ inside the expectation, which gives:

$$\begin{aligned} I_1 &= \mathbb{E}_{Y \sim Q(\cdot|\mathbf{X})} \left[-\log \left(\frac{\tilde{P}_\Phi(Y|\mathbf{X})}{P_\theta(Y|\mathbf{X})} \right) \right] = \underbrace{\mathbb{E}_{Y \sim P_\theta(\cdot|\mathbf{X})} \left[-\log \left(\frac{\tilde{P}_\Phi(Y|\mathbf{X})}{P_\theta(Y|\mathbf{X})} \right) \right]}_{\text{KL}(P_\theta(Y|\mathbf{X}), \tilde{P}_\Phi(Y|\mathbf{X}))} + I_2, \quad \text{where} \quad (37) \\ I_2 &= \mathbb{E}_{Y \sim Q(\cdot|\mathbf{X})} \left[-\log \left(\frac{\tilde{P}_\Phi(Y|\mathbf{X})}{P_\theta(Y|\mathbf{X})} \right) \right] - \mathbb{E}_{Y \sim P_\theta(\cdot|\mathbf{X})} \left[-\log \left(\frac{\tilde{P}_\Phi(Y|\mathbf{X})}{P_\theta(Y|\mathbf{X})} \right) \right]. \end{aligned}$$

By defining $g(Y) = -\log \left(\frac{\tilde{P}_\Phi(Y|\mathbf{X})}{P_\theta(Y|\mathbf{X})} \right)$ we have

$$\begin{aligned} |I_2| &\leq \sum_Y |g(Y)| \left| Q(Y|\mathbf{X}) - P_\theta(Y|\mathbf{X}) \right| \leq \|g\|_\infty \sum_Y \left| Q(Y|\mathbf{X}) - P_\theta(Y|\mathbf{X}) \right| \\ &\leq 2\|g\|_\infty \text{TV}(Q(\cdot|\mathbf{X}), P_\theta(\cdot|\mathbf{X})), \quad (38) \end{aligned}$$

where $\|g\|_\infty \triangleq \sup_{\mathbf{y}} |g(\mathbf{y})|$ is the infinite norm of the function g and $\text{TV}(Q(\cdot|\mathbf{X}), P_\theta(\cdot|\mathbf{X})) \triangleq \frac{1}{2} \sum_Y \left| Q(Y|\mathbf{X}) - P_\theta(Y|\mathbf{X}) \right|$ is the total variation between the distribution Q and P . Using $\epsilon < Q(\cdot|\mathbf{X})$ and $\epsilon < P_\theta(\cdot|\mathbf{X})$ we have $\|g\|_\infty \leq \log \left(\frac{1-\epsilon}{\epsilon} \right)$ resulting in:

$$|I_1| \leq \text{KL}(P_\theta(Y|\mathbf{X}), \tilde{P}_\Phi(Y|\mathbf{X})) + 2 \log \left(\frac{1-\epsilon}{\epsilon} \right) \text{TV}(Q(Y|\mathbf{X}), P_\theta(Y|\mathbf{X})) \quad (39)$$

Finally, combining (36),(37) and (39) yields the desired result. \square

F. Full Experimental Results

Here we provide the complete benchmark breakdown corresponding to the results summarized in Table 1 for Llama3.2-1B, Llama3.2-3B-Instruct, Llama3.1-8B-Instruct, Qwen3-1.7B, Qwen3-4B and Qwen3-8B. For each model, we report per-task zero-shot accuracies on ARC (Easy/Challenge), HellaSwag, WinoGrande, PIQA, BoolQ, and OpenBookQA under both MXFP4 and MXINT4 weight and activation quantization, comparing LATMiX to all reference baselines under the same experimental setup. Alongside the per-task scores, we report the average accuracy and the average recovery relative to the FP16 baseline. For both LATMiX and FlatQuant, the transformations were learned using WikiText2 dataset.

LATMiX: Learnable Affine Transformations for Microscaling Quantization of LLMs

Table 6. Performance of Llama-3.2-1B across weight and activation quantization configurations.

Format	Method	ARC-C	ARC-E	HellaSwag	WinoGrande	PIQA	BOOLQ	OBQA	Avg. Accuracy	Avg. Recovery (%)
MXFP4	FP16	36.86	61.70	65.79	62.75	74.81	63.82	37.00	57.53	100
	RTN	29.78	49.37	52.00	55.88	66.65	49.94	31.60	47.89	83.09
	QuaRot-RTN	28.24	48.40	47.84	55.72	66.54	59.54	31.40	48.24	83.38
	GPTQ	31.48	52.61	57.82	55.88	69.15	59.97	33.00	51.42	89.03
	QuaRot	33.36	54.76	56.92	59.12	69.91	59.60	33.60	52.47	91.09
	SpinQuant	31.83	54.08	55.87	55.33	68.50	61.96	32.80	51.48	89.20
	FlatQuant	30.89	55.56	58.57	57.93	69.26	62.14	32.80	52.45	90.54
	MR-GPTQ	30.97	55.13	58.33	56.12	70.62	62.17	34.40	52.53	90.89
	LATMiX-LU (Ours)	34.22	57.95	58.66	57.46	71.87	64.28	34.80	54.18	94.05
LATMiX-QR (Ours)	31.48	55.35	58.26	58.64	69.42	60.80	37.00	52.99	92.17	
MXINT4	RTN	26.54	42.05	44.29	53.12	62.84	56.97	30.20	45.14	78.14
	QuaRot-RTN	26.19	42.30	41.92	53.43	60.17	56.42	31.40	44.55	77.46
	GPTQ	31.31	50.80	53.37	56.75	66.16	54.62	30.40	49.06	85.00
	QuaRot	28.75	51.56	56.69	53.91	67.95	57.03	33.40	49.90	86.30
	SpinQuant	30.03	48.57	54.42	55.88	65.34	52.51	31.20	48.28	83.70
	FlatQuant	31.14	54.12	56.04	57.46	67.41	54.01	32.20	50.34	87.25
	MR-GPTQ	32.25	53.62	56.88	55.09	69.70	59.08	33.00	51.37	89.08
	LATMiX-LU (Ours)	32.94	58.04	58.27	56.59	69.31	61.80	35.20	53.16	92.40
	LATMiX-QR (Ours)	33.19	54.63	57.46	55.41	68.28	58.72	35.20	51.84	90.38

Table 7. Performance of Llama3.2-3B-Instruct across weight and activation quantization configurations.

Format	Method	ARC-C	ARC-E	HellaSwag	WinoGrande	PIQA	BOOLQ	OBQA	Avg. Accuracy	Avg. Recovery (%)
MXFP4	FP16	45.56	67.42	71.72	67.32	75.41	75.35	42.00	63.54	100
	RTN	38.05	59.97	66.87	62.98	72.25	75.05	36.80	58.85	91.76
	QuaRot-RTN	35.67	53.87	62.30	61.88	70.67	67.03	34.60	55.15	86.00
	GPTQ	39.93	61.32	69.15	63.93	72.85	72.78	36.80	59.54	92.97
	QuaRot	41.13	61.45	68.09	65.35	73.50	70.58	39.20	59.90	93.98
	SpinQuant	40.78	67.59	65.80	64.17	73.50	72.91	36.20	60.14	93.89
	FlatQuant	40.44	63.09	68.45	64.48	74.32	74.28	38.80	60.55	94.73
	MR-GPTQ	42.83	63.80	69.94	63.61	73.88	74.19	38.00	60.89	95.37
	LATMiX-LU (Ours)	43.09	65.07	68.87	64.40	74.65	78.29	41.40	62.25	97.75
LATMiX-QR (Ours)	43.00	65.53	69.09	64.88	75.08	75.20	38.00	61.54	96.30	
MXINT4	RTN	36.18	56.23	62.43	57.70	70.13	63.58	35.80	54.58	85.45
	QuaRot-RTN	31.57	50.76	56.66	56.43	68.44	65.14	30.80	51.40	79.71
	GPTQ	40.36	62.67	67.91	61.09	71.33	73.82	37.60	59.25	92.72
	QuaRot	41.21	61.15	68.05	60.22	73.01	70.34	36.40	58.63	91.76
	SpinQuant	38.74	52.90	63.89	62.12	70.18	70.43	33.80	56.01	87.41
	FlatQuant	39.25	58.54	66.06	63.93	72.03	74.13	34.20	58.31	90.77
	MR-GPTQ	43.09	64.90	68.69	63.85	73.39	73.61	38.20	60.82	95.34
	LATMiX-LU (Ours)	40.78	65.99	69.46	62.43	75.46	75.14	38.40	61.10	95.46
	LATMiX-QR (Ours)	39.93	64.06	66.03	65.19	72.91	74.25	36.00	59.77	93.21

Table 8. Performance of Llama-3.1-8B-Instruct across weight and activation quantization configurations.

Format	Method	ARC-C	ARC-E	HellaSwag	WinoGrande	PIQA	BOOLQ	OBQA	Avg. Accuracy	Avg. Recovery (%)
MXFP4	FP16	53.92	75.88	78.44	75.61	79.54	83.76	49.20	70.91	100
	RTN	48.55	71.17	74.99	70.48	77.58	81.10	44.00	66.84	93.77
	QuaRot-RTN	39.25	58.75	66.28	61.09	73.78	66.12	37.40	57.52	80.46
	GPTQ	49.15	73.99	76.14	71.59	78.24	81.44	46.20	68.11	95.70
	QuaRot	50.43	75.25	75.83	70.01	75.90	82.29	43.80	67.64	94.95
	SpinQuant	50.68	72.26	77.12	73.80	77.91	82.66	43.20	68.23	95.65
	FlatQuant	48.12	73.19	76.71	70.64	78.02	84.13	43.80	67.80	94.92
	MR-GPTQ	52.99	74.66	76.72	72.77	77.69	80.89	44.40	68.59	96.45
	LATMiX-LU (Ours)	50.09	72.85	76.99	71.98	78.89	84.37	46.20	68.77	96.58
	LATMiX-QR (Ours)	49.23	73.86	75.84	72.53	78.07	82.81	46.20	68.37	96.02
MXINT4	RTN	45.56	70.03	72.64	68.35	74.81	78.35	40.00	64.25	89.81
	QuaRot-RTN	44.62	68.64	70.59	63.14	74.76	78.01	40.80	62.94	88.11
	GPTQ	41.38	63.76	67.47	65.90	76.50	77.95	41.60	62.08	86.82
	QuaRot	49.06	71.25	76.66	69.85	77.58	80.83	44.60	67.12	94.24
	SpinQuant	49.91	75.97	74.93	71.35	78.62	78.10	45.80	67.81	95.39
	FlatQuant	46.33	71.25	75.03	70.32	77.42	80.12	41.80	66.04	92.35
	MR-GPTQ	50.77	74.07	75.99	70.48	78.18	81.99	45.80	68.18	95.87
	LATMiX-LU (Ours)	48.12	74.58	76.71	72.45	78.62	80.18	43.60	67.75	94.90
	LATMiX-QR (Ours)	46.93	73.53	76.67	71.43	77.64	82.84	43.60	67.52	94.47

Table 9. Performance of Qwen3-1.7B across weight and activation quantization configurations.

Format	Method	ARC-C	ARC-E	HellaSwag	WinoGrande	PIQA	BOOLQ	OBQA	Avg. Accuracy	Avg. Recovery (%)
MXFP4	FP16	43.17	69.57	60.17	60.38	72.20	77.61	37.20	60.04	100
	RTN	28.33	45.58	47.81	54.70	63.38	67.74	30.00	48.22	79.56
	QuaRot-RTN	28.16	40.28	43.19	55.56	61.64	63.49	27.60	45.70	75.47
	GPTQ	34.73	54.08	52.17	55.80	66.27	71.74	34.00	52.68	87.56
	QuaRot	35.84	52.57	53.69	55.64	66.27	69.33	35.60	52.71	88.11
	SpinQuant	33.36	57.70	55.31	56.12	66.49	72.54	33.20	53.53	88.55
	FlatQuant	36.69	57.58	56.04	57.06	68.72	74.07	33.80	54.85	90.98
	MR-GPTQ	33.96	55.60	52.62	54.85	66.59	70.52	34.00	52.59	87.34
	LATMiX-LU (Ours)	39.68	61.36	56.31	60.06	70.35	75.23	35.40	56.91	94.67
	LATMiX-QR (Ours)	37.37	61.70	55.47	57.46	68.99	76.79	36.40	56.31	93.56
MXINT4	RTN	26.11	39.06	42.74	49.88	59.03	63.18	28.80	44.11	72.98
	QuaRot-RTN	25.43	35.23	40.47	52.33	56.42	62.66	27.00	42.79	70.70
	GPTQ	31.14	48.61	49.21	52.01	63.49	64.25	30.60	48.47	80.42
	QuaRot	30.63	45.12	53.81	53.35	63.28	67.65	31.80	49.38	81.98
	SpinQuant	37.12	55.26	55.55	56.12	68.01	73.12	33.80	54.14	89.99
	FlatQuant	34.47	51.68	54.57	58.64	67.36	69.91	35.20	53.12	88.56
	MR-GPTQ	33.02	53.45	54.32	53.35	67.08	71.47	36.80	52.79	87.98
	LATMiX-LU (Ours)	36.01	60.10	56.32	56.67	68.17	73.73	33.00	54.86	90.77
	LATMiX-QR (Ours)	37.20	59.34	54.75	56.91	69.48	71.77	34.40	54.84	91.13

LATMiX: Learnable Affine Transformations for Microscaling Quantization of LLMs

Table 10. Performance of Qwen3-4B across weight and activation quantization configurations.

Format	Method	ARC-C	ARC-E	HellaSwag	WinoGrande	PIQA	BOOLQ	OBQA	Avg. Accuracy	Avg. Recovery (%)
MXFP4	FP16	53.50	78.41	70.02	67.01	74.97	85.02	40.20	67.02	100
	RTN	46.59	70.83	63.99	63.46	72.36	76.79	37.20	61.60	91.84
	QuaRot-RTN	41.30	68.98	59.35	61.72	70.29	80.15	36.40	59.74	88.66
	GPTQ	45.14	71.59	66.13	61.80	72.63	82.60	38.40	62.61	93.13
	QuaRot	45.31	69.95	63.90	62.90	71.11	80.40	35.60	61.31	91.00
	SpinQuant	43.00	73.32	63.52	62.27	70.84	80.98	39.00	61.85	92.04
	FlatQuant	46.84	70.37	64.87	61.96	72.63	82.78	37.80	62.46	92.96
	MR-GPTQ	45.31	68.73	64.15	64.25	72.14	83.76	36.00	62.05	92.02
	LATMiX-LU (Ours)	48.29	73.95	64.84	63.61	72.74	83.33	39.40	63.74	95.03
	LATMiX-QR (Ours)	48.55	74.07	65.98	63.38	73.67	83.73	38.80	64.03	95.33
MXINT4	RTN	33.70	49.33	54.44	54.22	67.74	63.58	34.40	51.06	76.47
	QuaRot-RTN	34.04	52.69	54.56	55.64	65.83	72.51	33.20	52.64	78.21
	GPTQ	40.78	60.23	61.23	62.27	70.84	65.08	38.60	57.00	85.78
	QuaRot	44.45	67.63	62.65	61.56	68.93	77.98	34.00	59.60	88.42
	SpinQuant	43.94	69.11	65.12	61.25	73.45	68.93	39.20	60.14	90.18
	FlatQuant	42.32	71.38	63.76	61.64	71.22	81.41	38.80	61.50	91.50
	MR-GPTQ	44.88	69.44	63.93	63.14	71.87	81.25	37.00	61.65	91.64
	LATMiX-LU (Ours)	46.42	70.45	66.36	63.93	73.39	78.44	38.80	62.54	93.35
	LATMiX-QR (Ours)	47.27	72.60	65.10	62.19	72.69	80.95	38.40	62.74	93.49

Table 11. Performance of Qwen3-8B across weight and activation quantization configurations.

Format	Method	ARC-C	ARC-E	HellaSwag	WinoGrande	PIQA	BOOLQ	OBQA	Avg. Accuracy	Avg. Recovery (%)
MXFP4	FP16	56.74	80.68	76.53	70.17	77.69	86.64	41.60	70.01	100
	RTN	45.14	69.32	69.25	65.59	73.23	80.00	38.20	62.96	89.69
	QuaRot-RTN	46.25	67.76	67.19	64.64	72.63	80.12	34.80	61.91	87.86
	GPTQ	49.57	75.00	70.62	65.59	74.59	83.76	40.60	65.68	93.77
	QuaRot	50.68	75.55	72.05	66.14	74.81	85.05	41.00	66.47	94.91
	SpinQuant	52.30	74.62	71.63	66.46	77.53	84.80	41.40	66.96	95.74
	FlatQuant	52.13	76.09	72.55	68.03	75.41	84.62	39.40	66.89	95.34
	MR-GPTQ	52.73	78.41	72.73	67.25	75.84	84.83	41.20	67.57	96.51
	LATMiX-LU (Ours)	54.69	77.57	74.06	69.93	76.33	85.81	42.20	68.66	98.24
	LATMiX-QR (Ours)	54.95	78.70	72.91	68.11	76.12	84.95	40.80	68.08	97.26
MXINT4	RTN	42.75	66.25	64.73	59.19	71.76	73.88	35.60	59.17	84.23
	QuaRot-RTN	40.70	65.45	65.38	61.88	72.47	74.62	34.20	59.24	84.01
	GPTQ	43.86	67.63	67.37	64.96	72.58	80.40	37.80	62.08	88.40
	QuaRot	50.77	75.13	71.09	67.48	75.24	81.50	38.00	65.60	93.42
	SpinQuant	50.43	71.38	73.11	65.90	75.68	82.02	39.80	65.47	93.51
	FlatQuant	48.55	74.92	70.98	67.01	75.57	83.76	39.80	65.80	93.76
	MR-GPTQ	49.15	74.24	72.01	68.82	75.79	83.27	40.40	66.24	94.51
	LATMiX-LU (Ours)	50.09	75.88	74.12	67.17	75.84	84.40	41.80	67.04	95.77
	LATMiX-QR (Ours)	52.73	76.01	71.23	67.25	76.39	83.24	39.60	66.64	95.09